Journal of Magnetic Resonance **143,** 329–351 (2000)
doi:10.1006/jmre.1999.1981, available online at http://www.idealibrary.com on IDEAL®

Comparison and Use of Vector and Quantum Representations of *J*-Coupled Spin Evolution in an IS Spin System during RF Irradiation of One Spin

M. Robin Bendall and Thomas E. Skinner*

The Russell Grimwade School of Biochemistry and Molecular Biology, University of Melbourne, Parkville 3052, Victoria, Australia; and
**Department of Physics, Wright State University, Dayton, Ohio 45435*

Received July 30, 1999; revised November 9, 1999

A comprehensive survey is provided of the analytical expressions for the orthogonal product operator states arising from any initial state of an IS *J*-coupled spin system during arbitrary RF irradiation of one spin. These equations exactly characterize the effect of *J* coupling during the application of the RF field. The survey differentiates two kinds of spin rotation, classical and nonclassical, where the second kind comprises any interconversion that includes the transverse two-spin coherence states, $2S_yI_x$ or $2S_yI_y$, as initial, transient, or final states, and the first kind comprises all other rotations. Classical rotations are defined as linear rotations of the nuclear spin magnetization vectors around effective fields and there is an exact correspondence between the resulting vector model and the quantum mechanical (QM) equations at all RF field strengths. The effect of scalar coupling can be neglected for $B_1 > 5J$. Nonclassical rotations are nonlinear in time for a constant RF field. At high field ($B_1 > 50J$), the effect of *J* modulation is negligible, and the rotation of magnetizations is classical to a very good approximation. At intermediate strengths ($5J < B_1 < 50J$), a semi-classical vector model of I-spin irradiation is applicable in which the *J*-coupled precession of the S spins is determined from a reduced coupling constant, but the effect of the S spins on the I spins is ignored (this model has previously been used to determine the effect of coupling during adiabatic pulses). At lower powers, the exact QM-derived equations must be used for nonclassical rotations, but continuous pictorial descriptions of the rotation of magnetizations determined from the vector sum of the product operator states are helpful in designing novel NMR applications. At all powers it is proven that the instantaneous reduced coupling constant acting on the S spins is $J\cos\phi$, where ϕ is the polar angle of the I-spin magnetizations, thus establishing the central tenet of the semi-classical model applicable at moderate power. Several spinstate transformations that combine the effects of RF and scalar coupling to produce the overall rotation can be generated in 100% yield using low power irradiation. Analogous transformations are also available using classical rotations and, in combination with their nonclassical counterparts, form a general class of frequency-selective pulses that we call *J* pulses. Any combination of a 90° pulse and a consecutive $(2J)^{-1}$ delay period can be replaced with a *J* pulse, and some initial approaches to designing shaped *J* pulses with improved offset profiles are explored. © 2000 Academic Press

Key Words: **IS spin system; *J* coupling; vector models; product operator states; *J* rotation matrices.**

1. INTRODUCTION

In a quantum mechanical analysis of the *J*-modulated behavior of weakly coupled I_mS_n spin systems during RF irradiation on one of the spins (*1*), a general means was provided for calculating exact analytical expressions for the evolution of the product operator states of the system. Except for a few fragmented studies detailed below, the complex effects of scalar coupling during RF pulses have been avoided: Most NMR experiments employ high-power square pulses so that coupling has a negligible influence ($B_1 \gg J$), and during soft frequency-selective pulses, *J* modulation is often eliminated by decoupling or spin locking (*2, 3*). However, scalar coupling has been shown to have a significant effect during adiabatic inversion pulses even when these are high-power broadband pulses. This *J* modulation can be described in terms of a straightforward semiclassical vector model (*4, 5*) and the results of the model are indistinguishable from full quantum mechanical (QM) calculations (*5, 6*). Insights gained from this physical model enabled the optimization of broadband adiabatic decoupling in terms of numerous experimental variables (*5–7*) and exposed the common error of expecting that no signal could be observed from decoupling antiphase or multiple quantum spinstates (*5, 6*). In this vector model it was assumed that the effective field $B_e \gg J$. Here we extend this research to calculate vectorial outcomes when B_e or B_1 is similar to or less than *J*, and in doing so a complete picture of spinstate transformations in an IS system is established.

It is often stated that a coupled IS spin system cannot be exactly described in terms of the evolution of magnetization vectors. But the result of any NMR experiment is detected via the oscillating electric currents induced in a coil by rotating nuclear magnetic fields in the sample. For NMR, the abstract machinery of quantum mechanics embraces reality by exactly

1090-7807/00 $35.00

predicting these macroscopic vectors. Since an NMR pulse sequence can be interrupted and the result measured at any time, QM calculations should be able to provide a continuous assessment of the evolution of these magnetizations. The existence of a closed set of analytical expressions for the product operator spinstates (*1*) leaves no doubt that this is so and that the calculations will be exact.

A detailed examination of this set of expressions shows that most RF-induced spinstate transformations correspond to simple classical vector rotations around effective fields that are the resultant of the coupling constant, resonance offset frequency, and RF field. In these cases a simple predictive vector *model* can be employed. However, at moderate and low RF powers, transformations including the antiparallel transverse spinstates, $2S_yI_x$, $2S_yI_y$, are nonclassical in the sense that they are not linear vector rotations around the vector sum of coupling, offset, and RF field. At moderate power, the predictive semiclassical *model* (*4, 5*) referred to above can still be used. But when the effective field is of the same order as *J*, the complex evolution of magnetizations must be calculated using the appropriate subset of QM-derived expressions (*1*). A vector *description* of the evolution is obtained by associating magnetization vectors with the product operator states. Even though such *descriptions* cannot quantitatively predict the path to some chosen final state, they may in favorable cases be used to indicate improvements or new variations of the initial experiment, by illuminating new aspects of spin physics. Accordingly, in this article, we draw a clear distinction between the terms vector *model* and vector *description:* the former are generally predictive via simple rules; the latter serve as a guide to new experiments that should be confirmed by exact calculation.

Classical IS rotations are analyzed in the next section. The general analytical expressions (*1*) are shown to include specific cases that have been previously published, and examples are given of new useful experiments, all in terms of a classical vector *model*. The general solution for the density matrix in terms of its orthogonal product operator components (*1*) facilitates a joint vector/QM picture of spin dynamics because these components are readily identifiable as the magnetization vectors that are potentially *measurable* in NMR experiments. In a third section we use the basis provided by the exact classical vector *model* to explore the concept of *measurability*. We conclude that, together with the QM-derived equations (*1*), this concept provides sufficient tools for the generation of the vector *descriptions* of nonclassical rotations. The prior literature in this area is limited and misleading so subsequent sections are devoted to a detailed analysis of nonclassical IS-spin transformations.

The result of this general analysis is a joint comprehensive QM and vector picture of classical and nonclassical IS-spin rotations under all possible conditions of RF irradiation on one spin. This illuminates numerous principles concerning the effects of *J* modulation during RF irradiation that should yield improvements in pulse sequence design. Indeed, any IS pulse sequence (not including simultaneous irradiation of both spins) can be completely described in terms of evolving magnetization vectors, and this should be of assistance to those practitioners who are not entirely comfortable with a purely abstract QM approach.

The study of IS spin systems subject to low RF power illuminates a general means of combining *J* modulation with frequency selectivity and thus a new class of selective pulses, dubbed "*J* pulses," is developed (*8*). Any combination of a 90° pulse and a $(2J)^{-1}$ free precession period in any pulse sequence can be replaced by a *J* pulse. The frequency response of these selective pulses can be improved by shaping the RF and the need arises to calculate the offset profile from time-varying RF inclusive of *J* modulation. By analogy with 3×3 rotation matrices for the three orthogonal cartesian components produced in the absence of coupling (*9*), the six orthogonal product operator components relevant to classical *J*-modulated rotations can be listed as a 6×6 "*J*-rotation matrix," and the four components for the nonclassical group yields a 4×4 *J*-rotation matrix. Listing the QM results in this way provides an obvious means of calculating the result of any shaped RF pulse by repetitive matrix multiplication and provides our general results in a concise but explicit form. Some initial approaches to shaping *J*-modulated pulses are explored in a final section of the paper.

The most straightforward pictorial explanations of the phenomena involved are sought, inclusive of prior vector models. The discussion is entirely in terms of an IS *J*-coupled group, but the general principles can be extended to I_mS_n spin-half systems. In the following it is assumed that the initial excitation is on the S spins and that the equilibrium I-spin magnetization has been eliminated by normal procedure (presaturation and/or phase cycling). The following treatment is applicable to any weakly coupled IS spin system subject to arbitrary conditions of *J* coupling, resonance offset, and RF irradiation of one spin (including homonuclear systems), but neglecting relaxation effects.

Standard product operator nomenclature is used (*10*), but we group all the one-spin operators, S_i ($i = x$, y, or z), together and describe them as in-phase magnetization, and we describe all the two-spin operators, $2S_iI_j$ ($i = x$, y, or z; $j = x$, y, or z) as antiparallel spinstates or magnetization. Sorensen *et al.* (*10*) further subdivided the two-spin operators as antiphase magnetization (e.g., $2S_xI_z$), two-spin coherence (e.g., $2S_xI_y$), and longitudinal two-spin order ($2S_zI_z$). We find that there is value in stressing the division into the two major groups of in-phase and antiparallel[1] spinstates because this directly yields the magnitude and orientation of the total *measurable* magnetization vectors.

[1] In recent work (*5, 6*) we sometimes referred to the second group as comprising "antiphase" spin states or magnetization, but this nomenclature may be confused with that for the subset, $2S_xI_z$ and $2S_yI_z$, as used by Sorensen *et al.* and many others, hence our change to the term, "antiparallel."

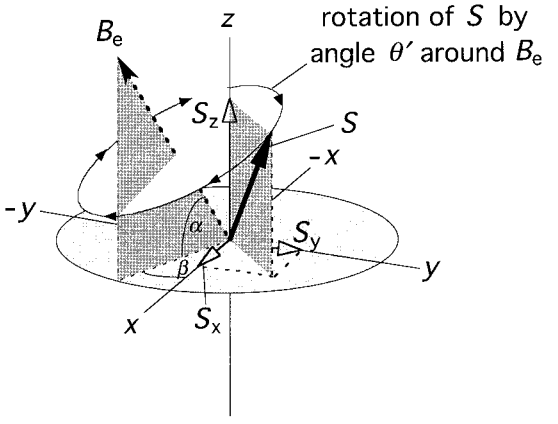

FIG. 1. Single spin rotation during a pulse of constant RF amplitude. Parameters are defined in Eqs. [1] to [14] for a single S-spin magnetization vector rotating around an effective radiofrequency field B_e for a pulse of length t. B_e is the resultant of ΔH along the z axis and the transverse B_1 field at a phase angle β to the x axis. Thus, the rotation is for a pulse of angle θ' about an axis which is rotated a phase angle β from the x axis and tilted upward by an angle α from the xy plane. Throughout this article, all fields are expressed in units of hertz (not radians) with the gyromagnetic ratio eliminated, and the orientation of effective fields is defined by an angle of tilt to the xy plane that is zero on resonance when $J = 0$ (not the polar angle).

2. CLASSICAL S-SPIN ROTATIONS

The simultaneous effects of S-spin irradiation and coupling to an I spin are examined with reference to the exact analytical equations (*1*) and pictorial representations of the rotating S-spin magnetizations. Several spinstate transformations that occur in 100% yield are described. The following brief recapitulation of single spin rotations establishes conventions. A minimal symbol set, as defined in the discussions of Figs. 1 and 2, is employed so that the trigonometric functions, f_A to f_G, defined in Eqs. [8] to [14], occur repeatedly throughout this work. Pulse and tilt angles are in radians (or degrees) and all other quantities are in units of seconds, or reciprocal time, or are dimensionless.

Single S Spin

It is well known that the torque on a magnetization vector of a single spin, subject to continuous uniform RF irradiation, is constant and proportional to the effective field, B_e, where B_e is the resultant of the RF field, B_1, and the resonance offset, ΔH (Hz). Defining B_1 as the reciprocal of the experimentally measured 360° pulse time on resonance,

$$B_e^2 = B_1^2 + \Delta H^2, \qquad [1]$$

or equivalently, as pictured in Fig. 1, the tilt angle α of the effective field relative to the xy plane of the rotating reference frame is

$$\sin \alpha = \Delta H/B_e, \quad \text{or} \quad \cos \alpha = B_1/B_e. \qquad [2]$$

On resonance, the magnetization will rotate around the RF field by an angle

$$\theta = 2\pi B_1 t, \qquad [3]$$

where t is the length of time the RF is applied, and off resonance the rotation is increased to

$$\theta' = 2\pi B_e t. \qquad [4]$$

An arbitrary rotation can be described in terms of a 3×3 rotation matrix to calculate the final orthogonal components of the S magnetization, S_j, from the initial components, S_j°:

$$\begin{bmatrix} S_x \\ S_y \\ S_z \end{bmatrix} = \begin{bmatrix} f_{xx} & f_{xy} & f_{xz} \\ f_{yx} & f_{yy} & f_{yz} \\ f_{zx} & f_{zy} & f_{zz} \end{bmatrix} \begin{bmatrix} S_x^\circ \\ S_y^\circ \\ S_z^\circ \end{bmatrix}, \qquad [5]$$

which in terms of linear combinations is

$$S_i = \sum_j f_{ij} S_j^\circ, \qquad [6]$$

where i and j take the values x, y, and z. Beginning with simple 3×3 matrices for rotations about the x, y, and z axes, in two straightforward steps it can be shown by basic mechanics (*9*) that the matrix for the arbitrary rotation defined in Fig. 1 is

$$f(\theta'[\beta], \alpha) = \begin{bmatrix} f_A\cos^2\beta + f_D\sin^2\beta & f_B - f_G\sin 2\beta & f_C\cos\beta + f_E\sin\beta \\ -f_B - f_G\sin 2\beta & f_A\sin^2\beta + f_D\cos^2\beta & -f_C\sin\beta + f_E\cos\beta \\ f_C\cos\beta - f_E\sin\beta & -f_C\sin\beta - f_E\cos\beta & f_F \end{bmatrix}, \qquad [7]$$

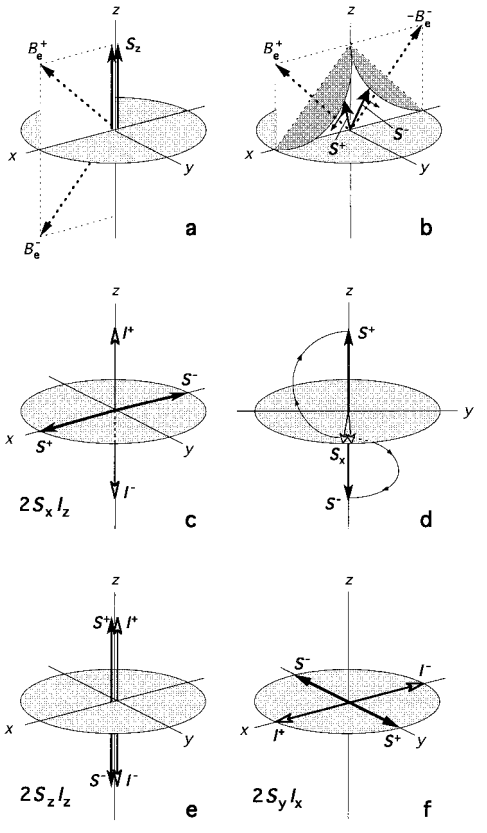

FIG. 2. Classical S-spin rotations in an IS spin system and vector depictions of product operator states. (a) In a coupled IS spin system the S spins experience two effective fields during RF irradiation, depicted as B_e^+ and B_e^-. For on-resonance RF of x phase, these fields are the resultants of B_1 along x and the coupling fields $+J/2$ and $-J/2$ along $\pm z$, respectively. On application of RF, the S_z magnetization splits into two equal vectors, S^+ and S^-, which rotate around B_e^+ and B_e^- in the normal classical manner. (b) If $B_1 = J/2$, B_e^+ and B_e^- have tilt angles of $\pm 45°$ to the x axis and S^+ rotates 180° clockwise around B_e^+ to align with the x axis after a time $t = (\sqrt{2}J)^{-1}$. S^- rotates clockwise about B_e^-, which can be more easily depicted as an anti-clockwise rotation about $-B_e^-$. (c) After the 180° rotation the spinstate is antiparallel $2S_xI_z$, also known as "antiphase x magnetization" (*10*). During the RF irradiation the I-spin magnetization vectors, I^+ and I^-, have grown from zero to maximum unit magnitude along $\pm z$ as discussed later with respect to Fig. 4. (d) Alternatively, if the same conditions are applied to initial S_x magnetization, clockwise rotations of 180° of $S^\pm$ around $B_e^\pm$ yield antiparallel $2S_zI_z$, shown in (e) and also called "longitudinal two-spin order" (*10*). (f) The vector depiction of the third type of antiparallel spinstate, $2S_yI_x$, also known as a "two-spin coherence" (*10*)—this is provided here for completeness and is discussed in Section 3.

where

$$f_A = \cos^2\alpha + \sin^2\alpha \cos\theta'; \quad [8]$$

$$f_B = \sin\alpha \sin\theta'; \quad [9]$$

$$f_C = \sin 2\alpha \sin^2[\theta'/2] = \sin\alpha \cos\alpha (1 - \cos\theta'); \quad [10]$$

$$f_D = \cos\theta'; \quad [11]$$

$$f_E = \cos\alpha \sin\theta'; \quad [12]$$

$$f_F = \sin^2\alpha + \cos^2\alpha \cos\theta'; \quad [13]$$

$$f_G = \cos^2\alpha \sin^2[\theta'/2] = (f_A - f_D)/2. \quad [14]$$

The sign convention is that clockwise rotations are positive and the x axis is clockwise of the y axis as in Fig. 1. Changing the sign of either of these changes the sign of all sine terms and thus all sin β and sin 2β terms in matrix [7] as well as the sign of f_C and f_E. For RF of x phase ($\beta = 0$),

$$f(\theta'[x], \alpha) = \begin{bmatrix} f_A & f_B & f_C \\ -f_B & f_D & f_E \\ f_C & -f_E & f_F \end{bmatrix}. \quad [15]$$

In the absence of an RF field, $B_e = \Delta H$, and all the terms in [15] are zero except $f_F = 1$, $f_A = f_D = \cos[2\pi\Delta H t_D]$, and $f_B = \sin[2\pi\Delta H t_D]$, which expresses the interchange of S_x and S_y magnetization via chemical-shift precession during time delay t_D.

Phase cycling a single rectangular pulse can be analyzed by changing β to $\beta \pm n*90°$ in matrix [7] and summing or subtracting the corresponding f_{ij} terms in the resulting matrices depending on the sign of the receiver phase. This eliminates some of the f_{ij} terms in the final 3×3 matrix and thus some orthogonal components of magnetization, and it demonstrates how the results of pulse sequences can be changed by phase cycling single pulses—examples are given in Ref. (*9*).

By digitizing shaped pulses into small time increments, each having constant attributes of amplitude and phase, matrix [7] can be used to calculate the time course and result of any frequency/amplitude-modulated pulse (since phase is the integral of frequency) by repetitive matrix multiplication. But the result of multiplying 3×3 matrices is a 3×3 rotation matrix, so the magnetization of a spin at a particular resonance offset has undergone an overall single rotation about some axis in 3D space and the logic concerning phase cycling applies to the overall shaped pulse. Thus, for example, if the f_{xy} term is eliminated for a rectangular pulse by phase alternation, it will also be eliminated for the complex pulse. These straightforward algorithms also apply to the 4×4 and 6×6 J-rotation matrices developed in the following sections.

Matrix [7] is a general analytical solution to the Bloch equations, neglecting relaxation—the only input from quantum mechanics is that there is an initial Boltzmann distribution producing a net magnetization. Rotation matrices explicitly reveal the rotation of this net magnetization in 3D space and can be extended to include scalar coupling as described below.

Irradiation of an S Spin Coupled to an I Spin

The first step in any heteronuclear pulse sequence is the excitation of the S spins prior to any RF on the I spins (apart

from presaturation), but this has received only modest attention for $B_1 \approx J$. Brondeau and Canet (*11*) investigated the transformation of S_z to $2S_xI_z$ under these conditions using a density matrix treatment and showed that the conversion was compatible with a simple vector model (*12*). Bazzo and Boyd (*13*) undertook a more general QM analysis to determine the exchange between the six spinstates, S_x, S_y, S_z, $2S_xI_z$, $2S_yI_z$, and $2S_zI_z$, via scalar coupling during selective pulses and summarized their analytical formulae in a 6×6 matrix. Below, this 6×6 matrix is derived from the 3×3 rotation matrix Eq. [15] using classical principles—it follows that **all** S-spin rotations during irradiation of the S spins are classical and an exact vector model is applicable.

The basis of the classical vector model is that one half of the S spins, S^+, are coupled to I spins aligned with the $+z$ axis (and rotate around an effective field B_e^+), and the other half, denoted by S^-, are coupled to I spins aligned with the $-z$ axis (and rotate around B_e^-). This is the only additional input from quantum mechanics and it is the same basic assumption made for the Heisenberg vector model (*14*). The magnitudes of these effective fields are

$$(B_e^{\pm})^2 = {B_1}^2 + [\Delta H \pm (J/2)]^2, \qquad [16]$$

in parallel with Eqs. [1] to [3]. On resonance, the magnitude of B_e^+ and B_e^- is identical, so $B_e^{\pm} = B_e^J = [{B_1}^2 + (J/2)^2]^{0.5}$ will be used.

The on-resonance S_z to $2S_xI_z$ conversion is shown in Figs. 2a to 2c to illustrate the two effective coupling fields and two of the possible spinstates. Matrix [7] can be applied to the individual rotations of S^+ and S^-, and the magnitudes of the six spinstates are determined by noting that in Fig. 2a, S_z is the sum of S_z^+ (the component of S^+ along z) and S_z^-, whereas in Fig. 2c, the antiparallel state, $2S_xI_z$, is given by S_x^+ minus S_x^-. Thus, scaling all vectors relative to unit positive magnitude, the orthogonal spinstates are given by

$$S_i = 0.5(S_i^+ + S_i^-) \qquad [19]$$

and

$$2S_iI_z = 0.5(S_i^+ - S_i^-), \qquad [20]$$

where i takes the values x, y, and z as usual.

Accordingly, the terms in the 6×6 matrices for the interconversion of the six spinstates can be written down by inspection since they are given by the sums and differences of the terms in the 3×3 matrices, [7] or [15], for rotations around B_e^+ and B_e^-. In general, listing the spinstates in the order, S_x, S_y, S_z, $2S_xI_z$, $2S_yI_z$, and $2S_zI_z$, the 6×6 matrices will be

$$f(\theta^{\pm}[\beta],\, \alpha^{\pm}) = 0.5 * \begin{bmatrix} \text{SUM of } 3 \times 3 \text{ matrix terms} & \text{DIFFerence of } 3 \times 3 \text{ matrix terms} \\ \text{DIFF.} & \text{SUM} \end{bmatrix}, \qquad [21]$$

where the diagonally opposite quadrants are identical. For example, defining $f^{\pm}$ as the appropriate member of Eqs. [8] to [14] with arguments $\alpha^{\pm}$ and $\theta^{\pm}$, the top-left term for the most general case resulting from matrix [7] is $(f_A^+ + f_A^-)\cos^2\beta + (f_D^+ + f_D^-)\sin^2\beta$, which simplifies to $f_A^+ + f_A^-$ for the 6×6 matrix resulting from Eq. [15] for RF of a single phase x:

$$f(\theta^{\pm}[x],\, \alpha^{\pm}) = 0.5 * \begin{bmatrix} f_A^+ + f_A^- & f_B^+ + f_B^- & f_C^+ + f_C^- & f_A^+ - f_A^- & f_B^+ - f_B^- & f_C^+ - f_C^- \\ -f_B^+ - f_B^- & f_D^+ + f_D^- & f_E^+ + f_E^- & -f_B^+ + f_B^- & f_D^+ - f_D^- & f_E^+ - f_E^- \\ f_C^+ + f_C^- & -f_E^+ - f_E^- & f_F^+ + f_F^- & f_C^+ - f_C^- & -f_E^+ + f_E^- & f_F^+ - f_F^- \\ f_A^+ - f_A^- & f_B^+ - f_B^- & f_C^+ - f_C^- & f_A^+ + f_A^- & f_B^+ + f_B^- & f_C^+ + f_C^- \\ -f_B^+ + f_B^- & f_D^+ - f_D^- & f_E^+ - f_E^- & -f_B^+ - f_B^- & f_D^+ + f_D^- & f_E^+ + f_E^- \\ f_C^+ - f_C^- & -f_E^+ + f_E^- & f_F^+ - f_F^- & f_C^+ + f_C^- & -f_E^+ - f_E^- & f_F^+ + f_F^- \end{bmatrix}. \qquad [22]$$

the tilt angles are

$$\sin\alpha^{\pm} = [\Delta H \pm (J/2)]/B_e^{\pm}, \quad \text{or} \quad \cos\alpha^{\pm} = B_1/B_e^{\pm}, \qquad [17]$$

and the rotation angles are given by

$$\theta^{\pm} = 2\pi B_e^{\pm} t, \qquad [18]$$

The corresponding J-rotation matrices for more than one coupled I spin can also be written down by inspection and the number of coupled S spins does not affect the progress of these classical rotations. For example, for an I_3S_n group the total S-spin magnetization splits into four components rotating around four effective fields which are the resultants of B_1, offset, and coupling fields $\pm J/2$ and $\pm 3J/2$.

Off resonance the rotations of S^+ and S^- are unequal, occurring about effective fields of different magnitude which

are not symmetrically tilted with respect to the *xy* plane as they are in Fig. 2a. An extreme example is described later in Fig. 3b. For large frequency offsets or for large B_1, the difference between B_e^+ and B_e^- approaches zero, S^+ and S^- follow identical paths, and J can be ignored. Thus when $J = 0$, or when B_1 or ΔH is large, the top-right and bottom-left quadrants of matrix [22] are all zeros and the other two quadrants reduce to 3×3 matrix [15]. Thus, there is no exchange of magnetization between S_i and $2S_iI_z$—this is the normal high-power approximation.

On resonance at lower power, $B_e^{\pm} = B_e^J$, $\alpha^+ = -\alpha^- = \alpha$, so Eq. [22] reduces to

$$f(\theta'[x],\ \alpha) = \begin{bmatrix} f_A & 0 & 0 & 0 & f_B & f_C \\ 0 & f_D & f_E & -f_B & 0 & 0 \\ 0 & -f_E & f_F & f_C & 0 & 0 \\ 0 & f_B & f_C & f_A & 0 & 0 \\ -f_B & 0 & 0 & 0 & f_D & f_E \\ f_C & 0 & 0 & 0 & -f_E & f_F \end{bmatrix}, \quad [23]$$

with $\theta' = 2\pi B_e^J t$. When both B_1 and ΔH are zero, all the terms in the 6×6 matrices are zeros except $f_A = f_D = \cos[\pi J t_D]$ and $f_B = \sin[\pi J t_D]$, which corresponds to free *J*-coupled precession interconverting $S_x \leftrightarrow 2S_yI_z$, and $S_y \leftrightarrow 2S_xI_z$ during delay t_D. This is easily demonstrated with the vector model of Fig. 2, but some additional nuances are discussed later in relation to Fig. 4. As noted for 3×3 rotation matrices, the elimination of some orthogonal spinstates by phase cycling can be analyzed by adding or subtracting 6×6 matrices for RF of different phase, and the results will be true for single rectangular pulses or shaped pulses simulated by repetitive matrix multiplication.

180^J Pulses: The $S_z \leftrightarrow 2S_xI_z$ and $S_x \leftrightarrow 2S_zI_z$ Transformations

The f_C term in the third column of matrix [23] corresponds to the on-resonance transformation of S_z to $2S_xI_z$ discovered by Brondeau and Canet (*11*) and illustrated in Figs. 2a to 2c. From Eq. [10], the transformation occurs in 100% yield when $B_1 = J/2$ ($\sin 2\alpha = 1$) and the rotation is 180° for a pulse length of $t = (\sqrt{2}J)^{-1}$. The f_C term in the fourth column of Eq. [23] determines the inverse transformation, $2S_xI_z \rightarrow S_z$, not previously described. The f_C terms in the first and last columns of matrix [23] reveal the new transformations, $S_x \leftrightarrow 2S_zI_z$, and the forward conversion is illustrated in Fig. 2d.

The time course of the spinstate transformations in Fig. 2 clearly demonstrate the contribution from *J* coupling during the pulse, a contribution which arises from the angle between B_e^+ and B_e^-. We will call the above matrices that include the effect of *J* modulation "*J*-rotation matrices," and we have named the corresponding RF pulses "*J* pulses," or more specifically 180^J or 90^J depending on the extent of the ideal rotation on resonance—the 90^J variety arises from nonclassical rotations as described in later sections. Recently we described potential uses of *J* pulses in multidimensional NMR (*8*) and further applications for the selective detection of infused labeled metabolites in *in vivo* NMR can be expected—it was shown in Ref. (*8*) that either a selective 90^J or a selective 180^J pulse can take the place of any combination of any hard 90° pulse and a consecutive $(2J)^{-1}$ free precession delay in any IS pulse sequence. A further advantage is that selective *J* pulses only increase the length of the normal $(2J)^{-1}$ period to $(\sqrt{2}J)^{-1}$, an increase of a modest 40% compared to conventional selective pulses.

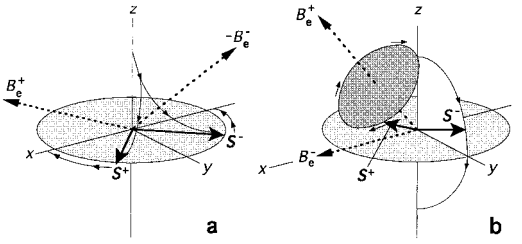

FIG. 3. Generalized 180^J rotations and the SPT method. (a) For $B_1 > J/2$ the tilt angle α of the effective fields on resonance, B_e^+ and B_e^-, is reduced compared to those shown in Fig. 2b. Consequently, during a period of constant RF irradiation, S^+ and S^- arrive at the *xy* plane before reaching the $\pm x$ axes. However, a period of coupled free precession, which is a fraction of $(2J)^{-1}$, will complete the spinstate transformation to $2S_xI_z$. (b) Selective irradiation at a resonance offset of $+J/2$ rotates S^- around the horizontal $B_e^- = B_1$ field. A 180° rotation to the $-z$ axis occurs after $t = (2B_1)^{-1}$ s. However, S^+ rotates around the tilted B_e^+ field ($= [B_1^2 + J^2]^{0.5}$) and is returned to the *z* axis to create the $2S_zI_z$ spinstate of Fig. 2e only if $B_e^+ = 2nB_e^-$. This defines particular values of $B_1 = J/(4n^2 - 1)^{0.5}$, where *n* is a positive integer.

The above 180^J pulses take the place of entire $(2J)^{-1}$ periods and are limited to selecting a single spectral bandwidth, of the order of *J*. This selected region can be expanded by increasing the pulse amplitude, decreasing the pulse length, and adding a delay before or after the pulse to complete the spinstate transformation as illustrated in Fig. 3a for $S_z \rightarrow 2S_xI_z$. Increased RF reduces the tilt angle α of the effective fields so that S^+ and S^- intersect the transverse plane without reaching the $\pm x$ axes. A delay period, t_D, which is a fraction of $(2J)^{-1}$, is required for S^+ and S^- to precess to $\pm x$, and the various parameters can be calculated for the on-resonance mechanism depicted in Fig. 3a. Defining $B_1 = bJ/2$, where $b \geq 1$, the calculation requires the application of matrix [23] for pulse time t_P beginning with unit S_z and then reapplication of the matrix for delay time t_D with $B_1 = 0$. Equating final $S_z = S_y = 0$ and $2S_xI_z = 1$, the three simultaneous equations readily yield

$$t_P = (\text{acos}[-1/b^2])/(\pi J(b^2 + 1)^{0.5}); \quad [24]$$

$$t_D = (\text{acos}[1/b])/(\pi J). \quad [25]$$

These equations provide the parameters for a 180^J spinstate transformation of any bandwidth greater than that provided by

$B_1 = J/2$. The equations are applicable to all four of the $S_z \leftrightarrow 2S_xI_z$ and $S_x \leftrightarrow 2S_zI_z$ conversions in any pulse sequence, although for the inverse transformation, $2S_xI_z \rightarrow S_z$, and the forward conversion, $S_x \rightarrow 2S_zI_z$, the free precession delay must precede the pulse as $\{t_D\text{–}180^J[S, t_P]\}$.

If the 180^J pulses are phase alternated (or appropriate pulsed gradients are employed), the $(f_E^+ - f_E^-)$ and $(f_C^+ + f_C^-)$ terms are eliminated from the phase-alternated equivalent of matrix [22], assuming concurrent alternation of receiver phase. The exact off-resonance selectivity of any general rectangular 180^J pulse is then given by

$$0.5[(f_E^+ + f_E^-)(b^2 - 1)^{0.5} + (f_C^+ - f_C^-)]/b. \qquad [26]$$

These $(f_E^+ + f_E^-)$ and $(f_C^+ - f_C^-)$ terms are from column 3, row 3, row 6, and column 6, respectively, of matrix [22] for $S_z \rightarrow 2S_xI_z$, $2S_xI_z \rightarrow S_z$, $S_x \rightarrow 2S_zI_z$, and $2S_zI_z \rightarrow S_x$, respectively. When $B_1 = J/2$, Expression [26] reduces to $0.5(f_C^+ - f_C^-)$ in agreement with the equation for the offset profile obtained in Ref. (*11*).

Selective Population Transfer: The $S_z \leftrightarrow 2S_zI_z$ and the Analogous $S_y \leftrightarrow 2S_yI_z$ Transformations

For a pulse of constant amplitude, the ideal 180^J rotation requires $B_1 = J/2$, and this is the lowest possible power for an effective *J*-modulated pulse on resonance. Below this level the tilt angles of $B_e^{\pm}$ in Fig. 2b are greater than 45° and the S^+ and S^- vectors do not ever reach the *xy* plane. A 100% spinstate transformation cannot be achieved. Further increases in selectivity may only be obtained by irradiating individual lines of a coupled multiplet as in the SPT method, also known as selective population inversion (*15*). In this technique a 180° pulse is first applied selectively to the S spins off resonance at either $-J/2$ or $+J/2$. This is equivalent to inverting either S^+ or S^- in Fig. 2a to produce the $-2S_zI_z$ or $2S_zI_z$ spinstate (Fig. 2e). The I-spin signal is then detected after a 90[I] pulse as $2I_yS_z$.

For initial S_z, the phase-alternated equivalent of matrix [22] (with no receiver alternation) has only two nonzero terms in column 3, $0.5(f_F^+ + f_F^-)$ for final S_z (row 3) and $0.5(f_F^+ - f_F^-)$ for final $2S_zI_z$ (row 6). For a 180° pulse at $+J/2$, $\Delta H = J/2$, $B_e^+ = (B_1^2 + J^2)^{0.5}$, $B_e^- = B_1$, $\sin \alpha^+ = J/B_e^+$, $\sin \alpha^- = 0$, $\cos \alpha^+ = B_1/B_e^+$, $\cos \alpha^- = 1$, and $t = (2B_1)^{-1}$. Setting $B_1 = J/a$ gives

$$0.5(f_F^+ - f_F^-) = 0.5\{(a^2 + \cos[\pi(a^2 + 1)^{0.5}])/(a^2 + 1) - \cos[2\pi B_1 t]\}. \qquad [27]$$

For SPT it was common to use a very selective low-power pulse such that $a > 10$ and Eq. [27] reduces to $\sin^2[\pi B_1 t] = 1$. However, with a knowledge of the exact spin physics, shorter, more efficient, 180° pulses can be found as drawn in the vector diagram of Fig. 3b. The $f_F^- = \cos[2\pi B_1 t]$ term in Eq. [27] is for the exact 180° rotation of S^- around the horizontal B_e^- axis, whereas the f_F^+ term is for the partial rotation of S^+ around the tilted B_e^+ axis. Clearly the overall transformation will occur in 100% yield if the latter rotation is n*360° so that $(a^2 + 1)^{0.5} = 2n$, or $a = (4n^2 - 1)^{0.5}$, with n a positive integer, giving a shortest pulse length of $\sqrt{3}(2J)^{-1}$ for $B_1 = J/\sqrt{3}$. Bildsoe (*16*) identified the $(4n^2 - 1)^{0.5}$ relation using a density matrix approach and numerical analysis. However, the exact selectivity profile of the SPT method, also given by $0.5(f_F^+ - f_F^-)$ as in Eq. [27], has not been established previously.

Other spinstate transformations can be derived from diagrams such as Figs. 2 and 3 or calculated from matrices [22] or [23]. For example, selective irradiation at $+J/2$ or $-J/2$ will induce the interconversion of S_y and $2S_yI_z$ in an analogous fashion to the SPT experiment, and the $f_D = \cos \theta'$ terms indicate that S_y and $2S_yI_z$ can be cleanly inverted on resonance at any RF field strength provided that the θ' rotation angle is calibrated to 180°. There are also several rotations which convert a pure spinstate to a 50:50 mixture of two other states or vice versa. All are potentially useful as building blocks in selective NMR.

3. VECTOR REPRESENTATIONS OF IS-SPIN EXPERIMENTS

A primary interest here is in the continuous *measurable* evolution of magnetization vectors in real space, not in nuclear spin evolution that takes place in abstract Hilbert or Louisville space. The knowledge gained of the path to any instantaneous state in real space may then be used for the purpose of design of new RF methods for NMR. Thus all magnetizations that are observable or potentially observable, i.e., *measurable*, are of concern. In the product operator formalism (*10*), spinstates have been described as observable if they directly provide detectable signal—for example, this did not include the S_z, $2S_yI_y$, or $2S_zI_z$ states. However, the concept of experimental *measurability* extends to each orthogonal IS spinstate, and any mix of these spinstates, within the definition that a state is *measurable* if maximum detectable signal can be observed directly, or is observable after a hard on-resonance pulse on the S spins and/or on the I spins.

For example, the $2S_xI_z$ state (Fig. 2c) is *measured* as directly observable antiphase S^+ and S^- signal at $+J/2$ and $-J/2$, respectively, whose magnitude sums to unity, compared to in-phase signal at $\pm J/2$ of total unit magnitude for S_x. The same applies to $2S_yI_z$ and S_y except for a phase shift of 90°. In contrast, potentially observable S_z and $2S_zI_z$ (Fig. 2e) may be *measured* by applying a hard 90[S] pulse in the first case to detect in-phase signal, or either a 90[S] or 90[I] pulse in the second case to observe the antiphase S signal or the antiphase I signal, respectively. (These hard 90° pulses must lie well within the high-power approximation discussed above in relation to matrix [22].) Similarly, antiphase I signals from $2S_xI_z$

and $2S_yI_z$ are *measurable* after a 90[S] pulse of *y* or *x* phase, respectively, and a 90[I] pulse of any phase. The transverse spinstates, $2S_xI_y$ and $2S_yI_y$, can be *measured* by a hard 90° pulse of appropriate phase on one spin and observation of the antiphase signal from the other spin. (The notion that such transverse states are unobservable or correspond to forbidden transitions harks back to the days of single channel spectrometers when it was technologically difficult to apply a discrete pulse to one nucleus and observe the other.) All NMR *measurements* are made after, or calibrated relative to, hard 90° pulses, and these hard pulses have themselves been calibrated experimentally by trial and error with respect to phase, frequency, and pulse length. There is no conceptual difference between observable and potentially observable spinstates.

Mixed spinstates, as in Fig. 2b, are the vector sums of individual spinstates. These, and in particular the resultant magnetization vectors S^+ and S^-, can be *measured* using fractional hard pulses of incremented phase. Assuming no knowledge of the prior experiment, two signals at $\pm J/2$ will be initially detected. Then, concentrating on the signal at $+J/2$, both the pulse angle and the phase of a hard S pulse at $+J/2$ could be varied by trial and error until pulse angle, ϕ, phase, φ, gives a maximum signal (S^+ transverse) and pulse angle, $90 - \phi$, phase, $180 - \varphi$, gives zero signal (S^+ along *z*). The 3D orientation of S^+ is then known unambiguously, and the procedure could be repeated at $-J/2$ to determine S^-. For arbitrary conditions, the experimentally *measured* orientations of S^+ and S^- can be resolved into the six possible spinstates, or the QM or vector calculation of the spinstates can be summed to determine S^+ and S^-. Thus there is a straightforward match between quantum mechanics, the classical vector model of the preceding section, and what is *measurable.* However the concept of *measurability* of the I-spin magnetization vectors in mixed spinstates requires further consideration with reference to previous vector pictures.

The Heisenberg vector *model,* which predated the popularization of the product operator (PO) formalism (*10*), was developed as a rigorous QM model in that magnetization vectors are physically identifiable with operators in the Heisenberg picture of quantum mechanics (*14*, *17*). Indeed, except for the PO spinstate nomenclature, and thus different vector labels (e.g., C_a and C_b in place of S^+ and S^-), this vector model depicted the antiparallel IS spinstates identically to the drawings in Fig. 2. More recently, Shriver (*18*) demonstrated that the PO states can be represented in this way as vectors in the Cartesian basis. However, a difference of convention exists between the pictorial representation used for the Heisenberg model and that of Shriver for in-phase transverse magnetization—in the former, $I^\pm$ vectors of unit magnitude were included along the $\pm z$ axis for the S_x or S_y picture, whereas these are absent in the latter. Inclusion of the $I^\pm$ vectors for in-phase magnetization combined two separate concepts that are explained below with reference to Fig. 4 for coupled free precession.

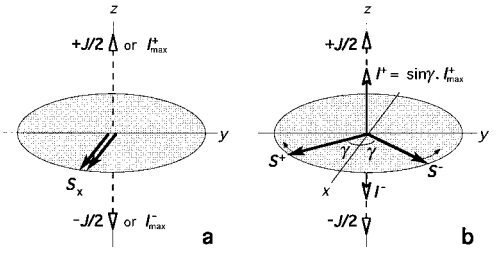

FIG. 4. Coupled free precession. (a) S_x is represented as two coincident magnetization vectors, S^+ and S^-, corresponding to the concept that a measurement of the S-spin signal is also a measurement of the probability of the I spins being found along $\pm z$. The vectors, I^+_{max} and I^-_{max}, represent this $\pm 1/2$ probability, or the $\pm J/2$ coupling fields of the I spins on the S spins, or the maximum potential length of the I-spin magnetization vectors that evolve when the S-spin vectors precess apart under the influence of the $\pm J/2$ fields. The *z* axis is the quantization axis, which is compared with that in Fig. 10a in later discussion. (b) During signal acquisition, or a pulse sequence delay, S^+ and S^- precess apart under the influence of the $\pm J/2$ fields and the angle γ is given by πJt. The I-spin magnetization vectors, I^+ and I^-, grow in proportion to sin πJt and are maximum and of unit magnitude equal to $I^\pm_{max}$ when S^+ and S^- are antiparallel, at which time the spinstate is $2S_yI_z$ (which is the same as the antiparallel state $2S_xI_z$ of Fig. 2c except for a 90° phase shift of the S-spin vectors).

First, in the Heisenberg model for free precession of initial S_x coupled to an I spin (*14*), these vectors represented the $\pm J/2$ coupling fields experienced by the S spins or, equivalently, that a measurement of the S signal at $\pm J/2$ is also a measurement of the equal probability of finding the I spins along $\pm z$. In Freeman's physical picture of multiple-quantum coherence (*19*) (similar to Ref. (*20*)), these vectors are called "*J*-vectors." In Shriver's representation, these fields are not depicted, but are implicit in that S_x is drawn as two vectors that will precess apart under the influence of coupling. In Fig. 4 we now label these fields as $\pm J/2$ and draw them as dashed vectors—they are equivalent to the $B_e^\pm$ effective fields of Fig. 2 with zero resonance offset ΔH.

Second, in the Heisenberg model these static I-spin vectors were called "polarization transfer vectors" (*17*) and it was shown that after a free precession period of $(2J)^{-1}$ s, when S^+ and S^- are antiparallel, they can be *measured* as antiphase I signal after applying a 90[S];90[I] pulse pair as in the above discussion of $2S_xI_z$ and $2S_yI_z$. However, within our present definition, they cannot be *measured* at time zero. This aspect is resolved by labeling them as $I^\pm_{max}$ in Fig. 4. The Heisenberg model demonstrated that at any time the antiphase I-spin signal, observable after a 90[S];90[I] pulse pair, is equal to $I^\pm_{max}\sin \pi Jt$, where $\sin \pi Jt$ is the proportion of S^+ and S^- that can be placed along $\pm z$ by the 90[S] pulse in agreement with a PO description.

The separation of these two concepts as in Fig. 4 improves the clarity of the pictorial model: The *measurable* I-spin vectors, I^+ and I^-, are depicted as growing in proportion to $\sin \pi Jt$. There is no *measurable* I-spin magnetization associated with in-phase S-spin magnetization. The total length of the $S^\pm$ and $I^\pm$ vectors in

Fig. 4 is given by the vector sum of the individual $S^{\pm}$ and $I^{\pm}$ vectors comprising the spinstates involved, S_x and $2S_yI_z$, and this is true for any classical rotation. This general rule is true because the six spinstates, transformed by the 6×6 *J*-rotation matrices, are orthogonal—this orthogonality arises naturally from density matrix theory (*1*, *18*). Thus the root-sum-of-squares of the terms in the columns of any of the 6×6 matrices must be unity or, in other words, beginning with a spinstate of unit magnitude, the total spinstate or vector sum must always be unity at any time independent of the complexity of the RF pulses applied. Furthermore, the *measurable* I-spin signal (the magnitudes of I^+ plus I^-) is the vector sum (root-sum-of-squares) of the antiparallel $2S_iI_z$ ($i = x$, y, and z) states, whereas the *measurable* S-spin magnetization (the magnitudes of S^+ plus S^-) is the vector sum of all spinstates. Stating this in alternate form, S^+ and S^- are of constant amplitude, whereas I^+ and I^- vary as sine of half the angle subtended by S^+ and S^-. The orientation of S^+, for example, is given by the vector sum of the S^+ portions of each pure PO spinstate, and the orientation and magnitude of I^+ are obtainable from the vector sum of the I^+ parts of all the pure antiparallel states.

The resulting pictorial vector *model* unambiguously illustrates the evolution of the *measurable* I-spin vectors. The addition of this I-spin evolution (as depicted in Fig. 4) to vector diagrams for classical S-spin rotations (as exemplified in Figs. 2b and 2d) provides an exact correspondence with all aspects of the 6×6 *J*-rotation matrices and completes the vector model of classical rotations. In the following sections, nonclassical IS-spin rotations that interchange four orthogonal spinstates are addressed. We have been unable to deduce the associated analytical equations on the basis of linear vector rotations. However, the general rule (and its subrules) that the *measurable* I- and S-spin vectors correspond to the vector sum of the four PO states holds true and provides a minimal but adequate representation. For example, experimental *measurements* of $I^{\pm}$ magnetizations in mixed spinstates, as described below, are similar to the above theoretical discussion of $S^{\pm}$ in mixed spinstates. Although the resulting vector *descriptions* are not readily predictive in all cases, because they depend on nonlinear rates of rotation, they are nevertheless helpful in many circumstances.

4. NONCLASSICAL I-SPIN ROTATIONS

In an IS-spin system, when the I spin is irradiated after excitation of the S spin, nonlinear, nonclassical rotations are induced for both spins.

Quantum Mechanical Analysis

The exact QM equations (*1*) show that such an NMR experiment interchanges four orthogonal spinstates. From Table 4 of Ref. (*1*), an explicit 4×4 *J*-rotation matrix can be written for these interconversions. Listing the spinstates in the order S_x, $2S_yI_x$, $2S_yI_y$, and $2S_yI_z$, the most general matrix is given by

$$f(\theta^{\pm}[\beta],\ \alpha^{\pm}) = 0.5* \begin{bmatrix} f_1 & f_2\cos\beta + f_3\sin\beta & f_2\sin\beta - f_3\cos\beta & f_4 \\ -f_2\cos\beta + f_3\sin\beta & f_5 + f_6\cos 2\beta & f_6\sin 2\beta + f_7 & f_8\cos\beta - f_9\sin\beta \\ -f_2\sin\beta - f_3\cos\beta & f_6\sin 2\beta - f_7 & f_5 - f_6\cos 2\beta & f_8\sin\beta + f_9\cos\beta \\ -f_4 & f_8\cos\beta + f_9\sin\beta & f_8\sin\beta - f_9\cos\beta & f_{10} \end{bmatrix}, \quad [28]$$

which, for an RF pulse of *x* phase, simplifies to

$$f(\theta^{\pm}[x],\ \alpha^{\pm}) = 0.5 * \begin{bmatrix} f_1 & f_2 & -f_3 & f_4 \\ -f_2 & f_5 + f_6 & f_7 & f_8 \\ -f_3 & -f_7 & f_5 - f_6 & f_9 \\ -f_4 & f_8 & -f_9 & f_{10} \end{bmatrix}, \quad [29]$$

where

$$f_1 = (1 + \cos[\alpha^+ - \alpha^-])\cos 0.5[\theta^+ - \theta^-] + (1 - \cos[\alpha^+ - \alpha^-])\cos 0.5[\theta^+ + \theta^-], \quad [30]$$

$$f_2 = (\cos\alpha^+ + \cos\alpha^-)\sin 0.5[\theta^+ - \theta^-] + (\cos\alpha^+ - \cos\alpha^-)\sin 0.5[\theta^+ + \theta^-], \quad [31]$$

$$f_3 = \sin[\alpha^+ - \alpha^-](\cos 0.5[\theta^+ - \theta^-] - \cos 0.5[\theta^+ + \theta^-]), \quad [32]$$

$$f_4 = (\sin\alpha^+ + \sin\alpha^-)\sin 0.5[\theta^+ - \theta^-] + (\sin\alpha^+ - \sin\alpha^-)\sin 0.5[\theta^+ + \theta^-], \quad [33]$$

$$f_5 = (1 - \sin\alpha^+\sin\alpha^-)\cos 0.5[\theta^+ - \theta^-] + (1 + \sin\alpha^+\sin\alpha^-)\cos 0.5[\theta^+ + \theta^-], \quad [34]$$

$$f_6 = \cos\alpha^+\cos\alpha^-(\cos 0.5[\theta^+ - \theta^-] - \cos 0.5[\theta^+ + \theta^-]), \quad [35]$$

$$f_7 = (\sin\alpha^+ - \sin\alpha^-)\sin 0.5[\theta^+ - \theta^-] + (\sin\alpha^+ + \sin\alpha^-)\sin 0.5[\theta^+ + \theta^-], \quad [36]$$

$$f_8 = \sin[\alpha^+ + \alpha^-](\cos 0.5[\theta^+ - \theta^-] - \cos 0.5[\theta^+ + \theta^-]), \quad [37]$$

$$f_9 = (\cos\alpha^+ - \cos\alpha^-)\sin 0.5[\theta^+ - \theta^-] + (\cos\alpha^+ + \cos\alpha^-)\sin 0.5[\theta^+ + \theta^-], \quad [38]$$

$$f_{10} = (1 - \cos[\alpha^+ + \alpha^-])\cos 0.5[\theta^+ - \theta^-] + (1 + \cos[\alpha^+ + \alpha^-])\cos 0.5[\theta^+ + \theta^-], \quad [39]$$

and $\sin\alpha^{\pm}$, $\cos\alpha^{\pm}$, and $\theta^{\pm}$ are defined in Eqs. [16] to [18]. On resonance, $\theta^+ = \theta^- = \theta'$, $\alpha^- = -\alpha^+ = -\alpha$, so the 4×4 matrix reduces to

$$f(\theta'[x],\ \alpha) = \begin{bmatrix} f_A & 0 & -f_C & f_B \\ 0 & 1 & 0 & 0 \\ -f_C & 0 & f_F & f_E \\ -f_B & 0 & -f_E & f_D \end{bmatrix}, \quad [40]$$

where the terms are given by Eqs. [8] to [13] and $\theta' = 2\pi B_e t$ in which $B_e = B_e^{\pm} = B_e^J$ as for the discussion following Eqs. [16] to [18]. The angle α is analogous to the residual on-resonance tilt of the effective field shown in Fig. 2 for classical rotations, arising from the $\pm J/2$ coupling fields, although, as described in subsequent sections, no classical rotations can be found around these individual tilted $B_e^{\pm}$ fields.

In the absence of an RF field, J-rotation matrix [40] reduces to

$$f(t) = \begin{bmatrix} \cos[\pi Jt] & 0 & 0 & \sin[\pi Jt] \\ 0 & 1 & 0 & 0 \\ 0 & 0 & 1 & 0 \\ -\sin[\pi Jt] & 0 & 0 & \cos[\pi Jt] \end{bmatrix}. \quad [41]$$

Columns 1 and 4 describe free J-coupled precession interconverting $S_x \leftrightarrow 2S_yI_z$, whereas columns 2 and 3 correspond to the well-known invariance of the transverse antiparallel $2S_yI_x$ and $2S_yI_y$ spinstates during time delays (*14*, *20*, *21*).

For large B_1, the high-power limit, or large ΔH, matrix [29] reduces to

$$f(\theta'[x],\ \alpha) = \begin{bmatrix} 1 & 0 & 0 & 0 \\ 0 & f_A & f_B & f_C \\ 0 & -f_B & f_D & f_E \\ 0 & f_C & -f_E & f_F \end{bmatrix}, \quad [42]$$

where J has been eliminated as insignificant and B_e in $\theta' = 2\pi B_e t$ is given by Eq. [1]. Note that the bottom right-hand corner of [42] corresponds to 3×3 matrix [15] rotating the antiparallel I-spin magnetizations.

An Experimental Measurement of the $S_x \rightarrow 2S_yI_y$ Nonclassical Rotation, Yielding a Vector Description

In parallel with the QM analysis, the disappearance of S_x during on-resonance CW irradiation of the I spins was investigated experimentally. At the time, the function f_1 (Eq. [30]), was known (*22*, *23*), reducing to f_A on resonance, and S_x goes to zero when $B_1 = J/2$ for a period of irradiation, $t = (2B_e)^{-1} = (\sqrt{2}J)^{-1}$. The study showed that a nonclassical vector evolution could be deduced experimentally, independent of quantum mechanics, so validating the literal view discussed above concerning the *measurability* of individual magnetization vectors associated with the PO states.

Writing out the f_1 function for the on-resonance condition with $B_e^{\pm} = B_e^J$,

$$f_A = \left(\frac{B_1}{B_e^J}\right)^2 + \left(\frac{J}{2B_e^J}\right)^2 \cos[2\pi B_e^J t]. \quad [43]$$

The effect of CW decoupling during signal detection is given by the Fourier transform of Eq. [43], yielding a centerband with amplitude, $1 - (J/2B_e^J)^2$ and sidebands at $\pm B_e^J$ with amplitude $0.5(J/2B_e^J)^2$. B_1 can be determined from the frequency difference between these sidebands, and $B_1 = J/2$ when the difference is $\sqrt{2}J$. This provides a convenient means of calibrating this low RF amplitude, and we have recently described several extensions to completely characterize the frequency, amplitude, and homogeneity of an insensitive I-spin channel by observing signals with a sensitive S-spin channel (*24*). In most of the following experiments the spins are also labeled as I≡^{13}C and S≡^{1}H to correspond to the matrix lists of spinstates as S_x and $2S_yI_j$.

Denoting a discrete on-resonance CW pulse on the I spins of length $(\sqrt{2}J)^{-1}$ and amplitude $J/2$, as a 90^J pulse (for reasons outlined below), with the S spins also on resonance, the sequence

$$90[\mathrm{S},\ -\mathrm{y}];\ 90^J[\mathrm{I},\ x];\ \text{acquire S} \quad [A]$$

generated no observable signal—note that Eq. [43] only ensures no in-phase S_x signal. Assuming that the original S magnetization must now be in one or more of the possible PO spinstates, the only possibilities are $2S_zI_j$ ($j = x$, y, or z), which is unlikely since the I spins and not the S spins were irradiated, or $2S_yI_x$ or $2S_yI_y$. Trial and error quickly showed that maximum antiphase S signal was returned by adding a hard 90[I] pulse as in

$$90[\mathrm{S},\ -y];\ 90^J[\mathrm{I},\ x];\ 90[\mathrm{I},\ \psi];\ \text{acquire S}, \quad [B]$$

where the phase, ψ, is $\pm x$, whereas zero signal was obtained if $\psi = \pm y$. The antiphase S signal at $\pm J/2$ was phase-shifted

90° from the S_x signal generated by the 90[S, $-y$] pulse, so the spinstate after the 90^J pulse was identified as pure $2S_yI_y$.

The addition of 90[S, x] to sequence [A] produced maximum antiphase I signal as in polarization transfer pulse sequences, so questions arise as to where do the I magnetizations come from, and how do they get to the $\pm y$ axes? Presumably they originate from the $\pm z$ axes, and it might be assumed by analogy with classical rotations (and has been in Ref. (*25*) as discussed later) that they rotate around tilted axes as in Fig. 2. The latter is not the case because it is impossible to transform antiparallel vectors along $\pm z$ to antiparallel along $\pm y$ via axes tilted at 45° since such tilts always interconvert antiparallel and in-phase vectors. Experimentally the question was resolved with the pulse sequence

$$90[\mathrm{S}, -y];\ a{*}90^J[\mathrm{I}, x];\ b{*}90[\mathrm{I}, \psi];\ \text{acquire S.} \quad [\mathrm{C}]$$

When the 90^J pulse was stopped part way through the conversion $S_x \rightarrow 2S_yI_y$, i.e., $0 < a < 1$, it was always possible to find a value of b between 0 and 1 such that when $\psi = -x$ maximum S-spin signal was regenerated. This ensured that the I-spin vectors had been returned to $\pm z$ by the reverse fractional hard pulse. Alternatively, a hard pulse of length $(1 - b)$*90° and phase $\psi = x$ generated fractional in-phase signal corresponding to the I-spin vectors being rotated down to the y axis of the transverse plane—the S signal associated with the partial precession of the S spins was removed as partial $2S_yI_y$. This proves that the I-spin vectors always lie in the yz plane, otherwise they could not be rotated perfectly to $\pm z$ and $\pm y$, respectively, with b*90° and $(1 - b)$*90° pulses of $\mp x$ phase, respectively.

The vector *description* of the 90^J pulse follows as in Fig. 5. The QM-derived matrix [40] confirms that the rotation axis of the I vectors is the x axis because on resonance the spinstate, $2S_xI_y$, is never produced. Detailed experimental information on the precession of the S^+ and S^- vectors was obtained from analyzing the S signals at $\pm J/2$ throughout the 90^J pulse using the sequence

$$90[\mathrm{S}, -y];\ a{*}90^J[\mathrm{I}, x];\ \text{acquire S,} \quad [\mathrm{D}]$$

where a was varied from 0 to 2. The total signal may be resolved into in-phase components along x, i.e., $S_x = 0.5(S_x^+ + S_x^-)$, and antiphase signal along y, i.e., $0.5(S_y^+ - S_y^-)$, as in Fig. 6. The latter can only be $2S_yI_z$ since $2S_yI_y$ is not directly observable. From the data in Figs. 6a and 6b,

$$S_x = \cos^2[\pi B_e^J t] = 0.5(1 + \cos[2\pi B_e^J t]), \quad [44]$$

in agreement with Eq. [43] for $B_1 = J/2$, and

$$2S_yI_z = (\sqrt{2}/2)\sin[2\pi B_e^J t]. \quad [45]$$

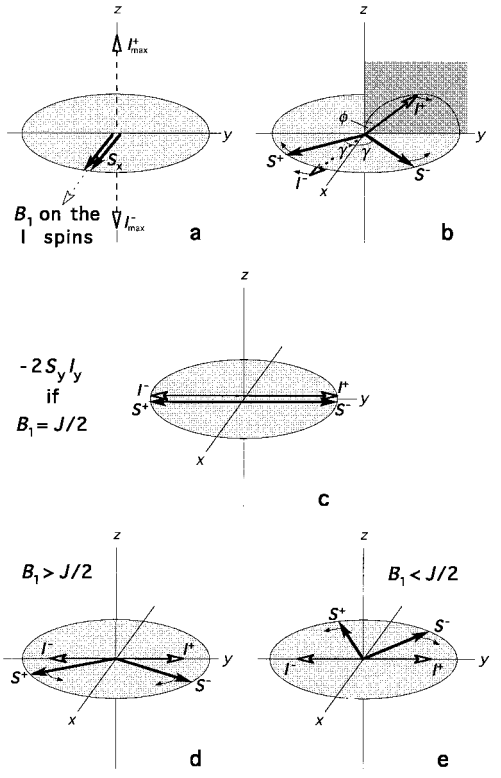

FIG. 5. The nonclassical rotation during a 90^J pulse on resonance. (a) The "virtual vectors," I^+_{max} and I^-_{max}, define the initial orientation and maximum amplitude of the I-spin magnetization vectors, I^+ and I^-, which evolve during I-spin irradiation. The axis of rotation of the I-spin vectors is the B_1 axis, not the $B_e^{\pm}$ axes as for classical rotations in Figs. 2 and 3. (b) During the applied RF, I^+ and I^- rotate around B_1 and increase in magnitude in proportion to sin γ as the S-spin vectors precess apart under the influence of coupling to the I spins. (c) If $B_1 = J/2$, I^+ and I^- obtain maximum unit magnitude at time $t = (\sqrt{2}J)^{-1}$ s after a rotation of 90°, and S^+ and S^- have also precessed 90°, but in opposite senses, to produce the pure antiparallel spinstate $2S_yI_y$ (which is the same as the antiparallel state $2S_xI_y$ of Fig. 2f except for a 90° phase shift of the S-spin vectors). If the RF irradiation is continued, S^+ and S^- reverse their direction of precession and refocus along x at $2t$. Meanwhile, I^+ and I^- continue to rotate around B_1 while decreasing in magnitude. They arrive at the $-z$ and $+z$ axes as their amplitude returns to zero. (d) If $B_1 > J/2$, the midpoint of a complete cycle ($\theta' = 180°$) differs from Fig. 5c in that I^+ and I^- have not reached maximum unit magnitude when their orientation is transverse, and S^+ and S^- have not precessed 90° when they stop and reverse direction. (e) If $B_1 < J/2$, at the cycle midpoint the situation is similar to Fig. 5d for I^+ and I^-, but S^+ and S^- have precessed more than 90°, although less than 180°, when they reverse direction.

In the spirit of the preceding section, the $2S_yI_y$ state can be *measured* by adding a hard 90° pulse on S or I to convert the spinstate to $2S_yI_z$ or $2I_yS_z$ as in

$$90[\mathrm{S}, -y];\ a{*}90^J[\mathrm{I}, x];\ 90[\mathrm{I}, \pm x];\ \text{acquire S}[\pm], \quad [\mathrm{E}]$$

or

$$90[\mathrm{S}, -y];\ a{*}90^J[\mathrm{I}, x];\ 90[\mathrm{S}, \pm x];\ \text{acquire I}[\pm], \quad [\mathrm{F}]$$

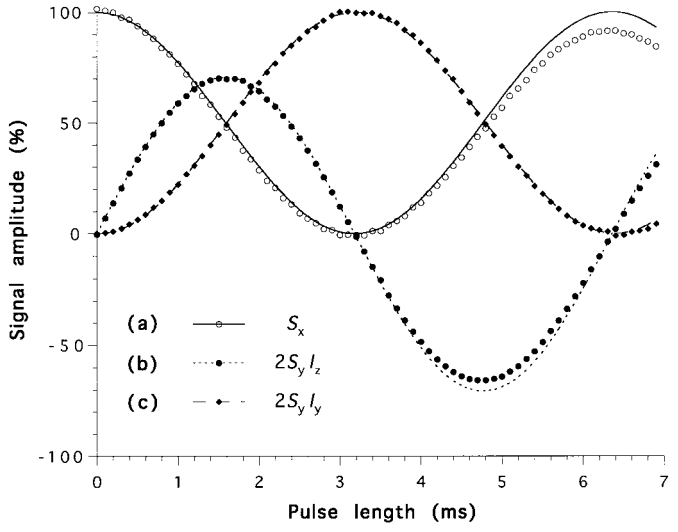

FIG. 6. Interchange of spinstates during I-spin irradiation with $B_1 = J/2$. (a) In-phase S_x signal, observed at $\pm J/2$ using pulse sequence [D], curve fitted to 100 $\cos^2[28.3*10^3t]$ ($R^2 = 0.99$). (b) Antiphase $2S_yI_z$ signal observed at $\pm J/2$ using pulse sequence [D] curve fitted to 70.7 $\sin[56.6*10^3t]$ ($R^2 = 0.99$). (c) Measurement of the $2S_yI_y$ spinstate by observing antiphase $2S_yI_z$ signal at $\pm J/2$ using pulse sequence [F] curve fitted to 100 $\sin^2[28.1*10^3t]$ ($R^2 = 0.999$). The x axis is the length of the I-spin irradiation. The arguments of the cosine and sine functions indicate a J value of 221.5 Hz from $\pi B_e^J = \sqrt{2}\pi J = 28.1*10^3$, compared to a spectral value of 222 Hz. B_1 was calibrated to within 1 dB of $J/2$ Hz using the method in Ref. (*24*) discussed in relation to Eq. [43]. Spectra were obtained using a standard HCN triple-resonance PFG probe on a 500-MHz Varian INOVA spectrometer using a 2% sample of the isopropyl ester of $H^{13}CO_2H$ in $CDCl_3$, doped with 0.2% $Cr(AcAc)_3$ relaxation agent.

respectively, where the phase alternations ensure elimination of undesired spinstates. The experiment in Fig. 6c for sequence [F], with the spin labels swapped to S≡^{13}C and I≡^{1}H, showed that

$$2S_yI_y = \sin^2[\pi B_e^J t], \qquad [46]$$

and the same experimental result was obtained from sequence [E] with I≡^{13}C and S≡^{1}H. Equations [45] and [46] agree with the f_B and f_C terms of the first column in matrix [40] when $B_1 = J/2$ (signs not determined experimentally) as further confirmation of the QM analysis and the vector *description.*

Some Aspects of Spin Physics

The Fig. 5 vector *description* of a 90^J pulse corresponds to the evolution of vectors in real space, since the orientation and magnitude of the S^+, S^-, I^+, and I^- magnetizations can be *measured* experimentally. With this experimental proof, vector *descriptions* of I-spin irradiation beginning with any of the other three spinstates can also be obtained with confidence directly from matrices [28], [29], or [40]. Some other general properties of nonclassical rotations are of great interest, as follows.

Nonlinear rotations. From Eq. [44] the precession angle, γ, of the S^+ and S^- vectors is given by

$$S_x = \cos\gamma = \cos^2[\pi B_e^J t], \qquad [47]$$

so the rate of precession induced by J coupling is not constant as it is in the classical examples of Figs. 2 and 4. The precession angle, ϕ, of I^+ and I^- may be calculated from Eqs. [44] to [46] or measured in additional experiments. The total of the antiparallel spinstates for Fig. 5b is sin γ, with the magnitude of $2S_yI_z$ as sin γ cos ϕ, and the magnitude of $2S_yI_y$ equal to sin γ sin ϕ. Thus

$$\sin\phi = \sin^2[\pi B_e^J t]/\sin\gamma \qquad [48]$$

and, again, unlike classical rotations, the rotation of the irradiated I spins is not linear. The rotation angles, γ and ϕ, may also be measured with reasonable accuracy using sequence [C] with $\psi = -x$. As noted above, the return of I^+ and I^- to the $\pm z$ axes ensures detection of all of S^+ and S^- so that the phase difference between these two signals at $\pm J/2$ equals 2γ, and ϕ can be determined from the fractional multiplier, b. However, ϕ can be measured with greater accuracy using a combination of sequences [C] and [E]:

$$90[\mathrm{S}, -y];\ a*90^J[\mathrm{I}, x];\ b*90[\mathrm{I}, -x];$$
$$90[\mathrm{I}, \pm x];\ \text{acquire S}[\pm]. \qquad [G]$$

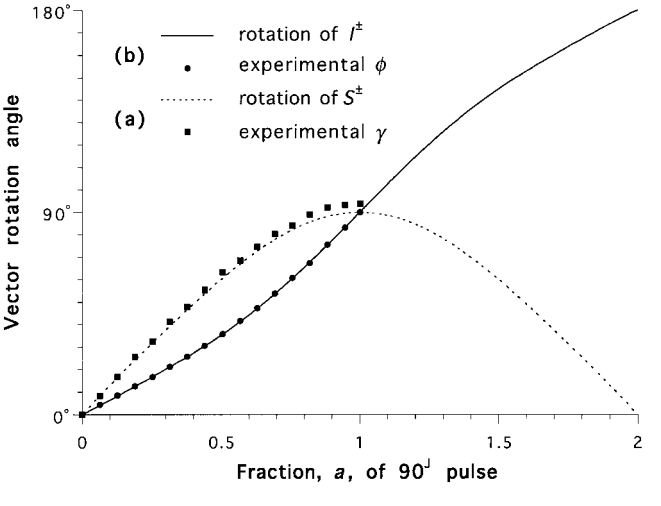

FIG. 7. Nonlinear rotations of I-spin and S-spin vectors. (a) Angle γ measured as half the phase difference between signals at $\pm J/2$ generated by sequence [C] when the b parameter is adjusted to provide maximum signal. The theoretical curve is acos{$\cos^2[a\pi/2]$} from Eq. [47]. (b) Angle ϕ measured by adjusting parameter b to obtain a signal null with sequence [G]. The theoretical curve is asin{$\sin^2[a\pi/2]/\sin\gamma$} from Eq. [48] assuming a theoretical value of γ from the curve in (a). Experiments were accomplished as described for Fig. 6.

When $b = 0$, fractional $2S_yI_y$ produced by the partial 90^J pulse is measured as $2S_yI_z$ as in sequence [E]. When b is adjusted to exactly reverse the ϕ angle, a signal null is obtained. The rotation angles measured in these ways are plotted in Fig. 7 in agreement with Eqs. [47] and [48].

Spinstate orthogonality. Despite fundamental differences, the orthogonality of the four spinstates ensures that there are some properties in common with classical rotations. A general rule of conservation of magnetization applies to unitary transformations and so, beginning with unit magnetization, the vector sum of all the spinstates is unity. Consequently, the sums-of-squares of the terms in each row or column of matrices [28], [29], [40], [41], and [42] is unity just as for the 3×3 and 6×6 matrices governing classical rotations. Magnetization does not disappear into forbidden QM space but is conserved. Thus, for nonclassical rotations, the I-spin signal (magnitude of I^+ plus I^-) is the vector sum (root-sum-of-squares) of the antiparallel $2S_yI_i$ ($i = x$, y, and z) states, and the total S-spin signal (magnitude of S^+ plus S^-) is the vector sum of all spinstates, as for classical rotations. Similarly, the alternate rules that S^+ and S^- are of constant amplitude, and I^+ and I^- vary as sine of half the angle subtended by S^+ and S^-, apply. The property of orthogonality also ensures that phase cycling, to eliminate signal from some spinstates, can be analyzed by adding or subtracting the corresponding terms in matrices for each phase in the same manner as for classical rotations.

The reduced coupling constant acting on the S spins. For the most general distribution of vectors that occurs on or off resonance, the transverse half angle γ and polar angle ϕ in Fig. 5b remain as useful parameters, with the $I^\pm$ pair twisted by some phase angle β about the z axis. The magnitude of the vector sum of the transverse antiparallel states, $2S_yI_x$ plus $2S_yI_y$, is now $\sin\gamma \sin\phi$, but importantly, the magnitudes of S_x and $2S_yI_z$ remain as $\cos\gamma$ and $\sin\gamma\cos\phi$, respectively. A central tenet of the semiclassical vector *model* applicable at moderate field strengths (discussed in Section 6) is that the instantaneous coupling constant acting on the S spins is $J\cos\phi$. Recasting this proposed theorem in terms of the instantaneous angular rate of precession of the $S^\pm$ vectors gives

$$d\gamma/dt = \pi J \cos\phi. \qquad [49]$$

Substituting the magnitudes of S_x and $2S_yI_z$ including the sign convention consistent with matrix [29] and Fig. 5 yields

$$d\{S_x\}/dt = \pi J\{2S_yI_z\}. \qquad [50]$$

If Eq. [50] is correct then from matrix [29] for initial S_x,

$$df_1/dt = -\pi J f_4. \qquad [51]$$

Expanding these functions using Eqs. [30] and [33] and eliminating the $\theta^\pm$ terms shows that for this to be true, two equations written as

$$(1 \pm \cos[\alpha^+ - \alpha^-])(B_e^+ \mp B_e^-) = J(\sin\alpha^+ \pm \sin\alpha^-) \qquad [52]$$

must be correct simultaneously for all values of $B_e^\pm$. Expanding the $\alpha^\pm$ functions demonstrates that this is so. Indeed, for each of the three other initial spinstates, the equations that parallel Eq. [51] are also true. Since the four spinstates are orthogonal, the theorem is proven for any mixture of spinstates and thus all possible conditions. Alternatively, Eq. [50] (and analogous equations governing the evolution of the three other spinstates) can be obtained most generally from the relation, $d\rho/dt = i[\rho, \mathcal{H}]$, where $\mathcal{H}$ in the system Hamiltonian in Ref. (*1*), and the density operator ρ is a linear combination of the four spinstates.

The effective field and the torque on the I-spin vectors. Equation [49] demonstrates that S^+ and S^- precess via a coupling that depends on the instantaneous orientation of the I-spin vectors relative to the z axis. But, returning to the on-resonance condition, there is nothing in the vector *description* of Fig. 5 to determine the rate of rotation of I^+ and I^- that must drive the vector evolution. For single spin magnetizations, the classical model derives from the torque induced on the magnetization by the RF field. From Eq. [48], $d\phi/dt$ indicates an instantaneous torque acting on the I-spin vectors equal to $B_1/(\cos\gamma + 1)$, which doubles from $B_1/2$ to B_1 during the 90^J pulse and averages $\sqrt{2}B_1/2$ compared to $B_e^\pm = \sqrt{2}B_1$. Thus the phenomenon is an interactive one in which the precession of the S spins passively depends on the orientation of the $I^\pm$ vectors, but the rotation of the I spins depends on the orientation of the $S^\pm$ vectors and the strength of the RF field.

The complex vector evolution off resonance. The I^+ and I^- vectors remain antiparallel under all conditions, otherwise more than four spinstates would be generated, but their motions are even more complex during off-resonance irradiation. Simulations using column 1 of matrix [29] for initial S_x indicate that the I^+ and I^- pair rotate around an axis whose orientation also varies with time producing spiral trajectories. For large offsets such that $B_e \approx B_e^\pm \gg J$, I^+ and I^- spiral from $\pm z$ and become spin-locked to the effective field B_e soon after application of the CW irradiation and the picture reduces to our previous vector *model* of decoupling—this is explored in greater detail in Section 6. However, in general it is impossible to draw a predictive *model* for off-resonance irradiation when $B_1 \approx J/2$ and simulations using matrix [29] are necessary. In all cases at low B_1, on and off resonance, the *measurable* I-spin magnetizations do not rotate around constant effective fields and this negative property is independent of the initial spinstate. For classical IS rotations, individual terms in the 6×6 matrices are either sums or differences of terms for single vector rotations, e.g., $\sin\alpha^+\sin\theta^+ \pm \sin\alpha^-\sin\theta^-$. In comparison, the individual nonclassical terms such as f_4 in Eq. [33]

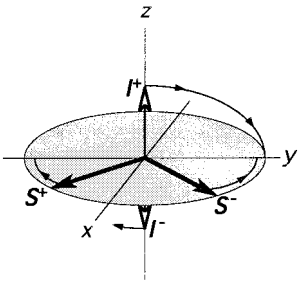

FIG. 8. Generalized 90^J pulse. A period of coupled free precession as in Fig. 4 produces a mixture of S_x and $2S_yI_z$ magnetization. As described in the text, it is possible to calculate an RF field, $B_1 > J/2$, and pulse length such that the I^+ and I^- magnetization vectors rotate to the $\pm y$ axes during the pulse in the same time as S^+ and S^- precess to $\mp y$ to produce pure $-2S_yI_y$ magnetization.

are both sums and differences, and the rotation angle arguments, θ^+ and θ^-, are added and subtracted instead of the trigonometric terms. This is the mathematical expression of the entanglement of the I and S spins that provides the complexity of the spin physics off resonance. The collapse of $0.5[\theta^+ - \theta^-]$ to zero and $0.5[\theta^+ + \theta^-]$ to θ' on resonance, yielding 4×4 matrix [40], permits the simple vector picture of Fig. 5 and generates the same trigonometric functions as in the 6×6 matrix [23] for on-resonance conditions. At least in part, these parallels ensure that there are 100% spinstate transformations for nonclassical rotations analogous to the classical conversions already described in Section 2.

5. SPINSTATE TRANSFORMATIONS USING NONCLASSICAL ROTATIONS

The 90^J Pulse, the $S_x \leftrightarrow 2S_yI_y$ Transformation, and Continuous Uniform I-Spin RF Applied on Resonance to Initial S_x

As noted in Section 2, it has been shown that either a frequency-selective 180^J or a 90^J pulse can take the place of any consecutive combination of a hard 90° pulse and a $(2J)^{-1}$ free precession delay in any pulse sequence (*8*), and either substitution increases the overall length of the delay by a modest 40% to $(\sqrt{2}J)^{-1}$. Classical 180^J pulses are restricted to excitation and polarization transfer steps, whereas 90^J pulses involve the transverse antiparallel $2S_xI_y$ or $2S_yI_y$ states and so are restricted to polarization transfer and multiple quantum steps. In triple resonance pulse sequences it is possible to entirely nest a 90^J pulse (but not a 180^J pulse) in a long free precession period determined by an independent shorter coupling constant. This completely avoids increasing the time length of the pulse sequence even though the frequency of one nucleus has been restricted to a bandwidth of the order of J (*8*).

As for 180^J pulses in Section 2, the bandwidth of 90^J pulses can be increased by increasing the RF amplitude, decreasing the pulse length t_P, and adding a delay t_D. If the RF amplitude is increased to $bJ/2$, where $b \geq 1$, the I^+/I^- vectors of Fig. 5b rotate faster and arrive at the transverse plane before the S^+/S^- vectors have precessed to the y axes, as depicted in Fig. 5d. It might seem that a short delay would enable S^+/S^- to precess the remaining distance. They do, but the final result is not the required one—from Fig. 5d or matrix [40], the system is a mixture of only S_x and $2S_yI_y$ after the pulse and from Fig. 4 and matrix [41], S_x can only precess to $2S_yI_z$, and $2S_yI_y$ is invariant. However, if the delay is imposed first as in Fig. 8, the value of b necessary to rotate I^+/I^- to the xy plane in the time necessary for S^+/S^- to precess to the y axes can be determined from matrices [40] and [41]. The derivation of the equations for t_p and t_D for a generalized 90^J pulse is similar to that described in Section 2 for 180^J pulses. Indeed, with the forward and reverse conversions for $S_x \leftrightarrow 2S_yI_y$ enabled as $\{t_D–90^J[I, t_p]\}$ and $\{90^J[I, t_p]–t_D\}$, respectively, the pulse and delay times are exactly determined by Eqs. [24] and [25] of Section 2. However, off resonance, signal intensity follows a different equation to that for the 180^J transformations and is given by

$$0.5[f_9(b^2 - 1)^{0.5} + f_3]/b. \qquad [53]$$

This equation is discussed in Section 7 in comparison to shaped 90^J pulses.

The facile invention of generalized rectangular 90^J pulses beginning with a proposed vector diagram illustrates the value of the on-resonance *descriptions* of the type given in Figs. 5 and 8. In actuality, these vector pictures and their confirmation preceded the development of the analogous generalized 180^J case. On-resonance vector *descriptions* for continuous RF of any amplitude applied to initial S_x can also be obtained from the first-column terms of matrix [40]. For all values of B_1, S^+/S^- always reverse midway through each cycle, depicted in Figs. 5c, 5d, and 5e, to refocus to pure S_x when the rotation of I^+/I^- is 180° at $\theta' = 360°$. The cycle begins again from Fig. 5a. Although I^+/I^- terminate along the $\mp z$ axes but originate along $\pm z$, this transition at the end of each cycle is not discontinuous because I^+/I^- are of zero magnitude at this time. For $B_1 > J/2$, S^+/S^- do not reach the $\mp y$ axes by the time I^+/I^- are transverse—the system is a mixture of S_x and $-2S_yI_y$, so I^+/I^- are less than unit magnitude, as shown in Fig. 5d. For very large B_1, the precession of S^+/S^- during the RF reduces to zero and, at the midpoint of the rotation, I^+/I^- are vanishingly small (the high-power approximation). For $B_1 < J/2$, S^+/S^- have precessed past the $\mp y$ axes at the midpoint of each cycle as in Fig. 5e, and again I^+/I^- are less than unit magnitude because the system is a mixture of $-S_x$ and $-2S_yI_y$. The S^+/S^- vectors never precess as far as the $-x$ axis before reversing their motion, except in the limit of $B_1 \rightarrow 0$ in which case the vector motion becomes continuous free precession. Pure $-2S_yI_y$ is only produced for the specific case of $B_1 = J/2$.

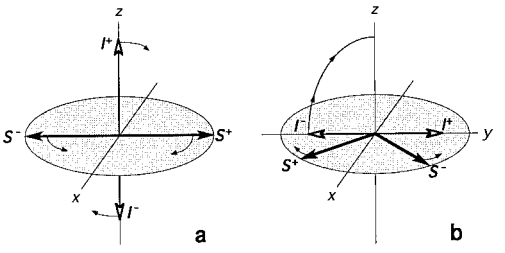

FIG. 9. General description for on-resonance RF applied to initial $2S_yI_z$. (a) The I^+ and I^- vectors rotate around the x axis, the axis of application of the B_1 field, and decrease in magnitude as the initially antiparallel S^+ and S^- vectors precess toward each other. (b) At $\theta' = 90°$ $I^{\pm}$ are transverse and have reached their minimum size. At this point the $S^{\pm}$ vectors reverse their direction of precession to return to the $\pm y$ axes, but $I^{\pm}$ continue rotating in the same direction increasing in size until they are of unit magnitude and inverted along the z axes. If the RF is continued from $\theta' = 180°$ to 360° the picture is the same except that $S^{\pm}$ precess toward the $-x$ axis and reverse, and $I^{\pm}$ rotate through the $\mp y$ axes. At very low power, S^+ and S^- almost reach the $\pm x$ axes at $\theta' =$ 90° and 270° and I^+ and I^- become vanishingly small.

Irradiation of One Multiplet Line: The $S_x \leftrightarrow 2S_yI_x$ and the Analogous $2S_yI_z \leftrightarrow 2S_yI_y$ Transformations

Further complexity is added for off-resonance irradiation. For example, the outcome for initial S_x is given by the first-column elements of matrix [29] rather than matrix [40] for the on-resonance case. However a simplification might be expected at $\Delta H = J/2$ where $B_e^+ = (B_1^2 + J^2)^{0.5}$ and $B_e^- = B_1$. In particular, $2S_yI_x$ is generated off resonance from initial S_x and, putting $B_1 = J/a$, the equation for this spinstate simplifies as

$$2S_yI_x = -0.5f_2 = \cos[\theta^+/2] = \cos[(1 + a^2)^{0.5}\pi/2], \quad [54]$$

when $\theta^- = \pi$, i.e., $t = (2B_1)^{-1}$. The transformation is obtained in 100% yield for $a = (4n^2 + 1)^{0.5}$, n a positive integer. There is a remarkable parallel with the classical SPT experiment in that $B_1 = J/\sqrt{3}$, $J/\sqrt{15}$, $J/\sqrt{35}$, $J/\sqrt{63}$, . . . , gives maximum conversion, but Eq. [54] differs from [27] providing alternating $\pm 2S_yI_x$ with incremented n. The frequency profile, given by the function $-0.5f_2$, also differs. These solutions illustrate the complexities off resonance. For example, for $B_1 = J/\sqrt{35}$, the I^+/I^- pair originates on $\pm z$ as usual and rotates 1.25 revolutions around the z axis, passing twice through the transverse plane, to arrive at $\pm x$ after $t = (2B_1)^{-1}$. The rotation around z increases by an extra 0.5 revolutions for each increment of n.

The conversion $2S_yI_z \leftrightarrow 2S_yI_y$ is similar to the $S_x \leftrightarrow 2S_yI_x$ transformation. Beginning with the $2S_yI_z$ state, the yield of $2S_yI_y$ is given by $0.5f_9$ for irradiation at $J/2$, which reduces to Eq. [54] under the same conditions.

Continuous Arbitrary I-Spin RF Applied on Resonance to Other Initial Spinstates

Vector *descriptions* of the outcome of RF applied to any of the other three spinstates can be generated as for initial S_x in Fig. 5. Some examples have already been included above as the reverse transformations e.g., $2S_yI_y \rightarrow S_x$. On-resonance irradiation of $2S_yI_z$ is of interest for comparison with the moderate power vector *model* discussed below. A vector *description* is readily generated using the terms in column 4 of matrix [40] and is drawn in Fig. 9. There is no special case for $B_1 = J/2$ as there is for initial S_x. In all cases the precession of S^+/S^- reverses at times given by $\theta' = 2\pi B_e t = (2n + 1)*90°$ (n an integer) and becomes antiparallel again at $n*180°$. At high RF power the precession of S^+/S^- becomes vanishingly small and the system oscillates between $2S_yI_z$ and $2S_yI_y$ (the high-power approximation). With decreasing RF, S^+/S^- have precessed further at $\theta' = (2n + 1)*90°$, but never quite converge on the x axis except in the limit of $B_1 \rightarrow 0$ in which case the vector motion becomes coupled free precession. The rotation of I^+/I^- is continuous, in propeller fashion, but nonlinear in time, revolving once for $\theta' = 360°$.

For initial $2S_yI_x$, the I-spin magnetization vectors remain locked along the B_1 x axis despite the contribution of the $\pm J/2$ coupling fields of the S spins to the effective fields. This invariance to RF irradiation is given by the term of unity in column 2 of matrix [40] with all other terms zero.

Initial $2S_yI_y$, given by the terms in column 3 of matrix [40], provides the most complex vector *description* of the four initial spinstates and, to conserve journal space, has not been drawn here. However a complete cycle occurs for every $\theta' = 360°$ (as for initial S_x and $2S_yI_z$) and it is notable that when $B_1 < J/2$ the $I^{\pm}$ vectors reverse their direction of precession twice during each cycle. This double reversal of the rotation of the I-spin vectors at low RF amplitude provides significant evidence against the notion that these rotations could be explicable in terms of a classical torque.

6. PREVIOUS STUDIES OF NONCLASSICAL ROTATIONS AND APPROXIMATIONS AT HIGH AND MEDIUM FIELD STRENGTH

There have been few previous studies of RF-induced rotations that include the transverse antiparallel states $2S_yI_x$ and $2S_yI_y$. Some are in error and all are misleading in that the different effects at high, medium, and low RF power have not been adequately addressed. A quantitative analysis of the various results available from the QM-derived matrix [29] now shows that there are four important regimes: high RF power with $B_1 > 50J$; medium RF corresponding to $50J > B_1 > 5J$; low RF for which $B_1 < 5J$; and $B_1 = 0$.

High RF Field Strength, $B_1 > 50J$, and the High-Power Approximation

In their study of the illusions of spin decoupling, Levitt *et al.* (*26*) showed that a variable period of CW decoupling applied to spinstate S_x prior to signal acquisition had no effect on the final signal. As a counterexample they applied the same experiment to initial $2S_yI_z$ magnetization and noted that the system oscillated between this initial spinstate and $2S_yI_y$ according to

$$\cos[2\pi B_1 t]\{2S_yI_z\} - \sin[2\pi B_1 t]\{2S_yI_y\}. \qquad [55]$$

However, their work was based on the premise that B_1 should be "sufficiently strong." Although presumably not intended for CW decoupling, this premise corresponds to the high-power approximation summarized above in the form of matrix [42], which on resonance reduces to

$$f(\theta[x]) = \begin{bmatrix} 1 & 0 & 0 & 0 \\ 0 & 1 & 0 & 0 \\ 0 & 0 & \cos[2\pi B_1 t] & \sin[2\pi B_1 t] \\ 0 & 0 & -\sin[2\pi B_1 t] & \cos[2\pi B_1 t] \end{bmatrix}. \qquad [56]$$

With a trivial change in sign convention, Expression [55] is identical to the terms in column 4 of [56], and the invariance of initial S_x is given by column 1. Beneath the layer of phenomena observed by Levitt *et al.* lies two other nonillusory layers corresponding to medium and low B_1 power. To avoid a 1% error for a $^{13}C^1H$ spin system, the CW RF applied to initial $2S_yI_z$ must have an amplitude of more than 7.5 kHz, otherwise signal in the form of S_x will be observed during decoupling (calculated from column 4 of matrix [40]). In broadband adiabatic decoupling, 5% sidebands are easily generated from this source (*6*). Setting the lower boundary of the high-field approximation to $50J$ limits simulation or spectral errors to less than about 1–5%.

It is now well-known that the conditions expressed in matrix [56] are sufficiently extreme as to provide our ability to precisely *measure* the "unobservable" $2S_yI_y$ state by applying a hard 90° pulse to convert the spinstate to $2S_yI_z$ as mentioned in Section 3, above. This conversion is given by the sine term in column 3 of [56].

Medium RF Field Strength, $50J > B_1 > 5J$, and the Vector Model of Nonclassical Rotations

RF of moderate power is most commonly encountered in decoupling schemes, broadband adiabatic pulses, and selective broadband pulses. Typical descriptions of the mechanisms underlying decoupling methods assume that the RF instantaneously changes the state of the spin to which it is applied, so that coupling evolution proceeds with strength J in one direction (before the spinstate flips) and then reverses and refocuses after the spin is instantaneously inverted (*27*). The effect of RF on the strength of the coupling modulation is ignored and this is a poor approximation when the cycle time of the spin inversions are significant compared to J as in adiabatic decoupling. For CW decoupling, the detailed analysis by Anderson and Freeman (*22*) for all power levels indicated that the concept of spin flips is unnecessary, so there appear to be two separate mechanisms for decoupling.

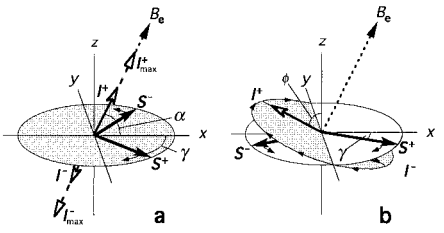

FIG. 10. Off-resonance vector *model* of I-spin irradiation. (a) For initial S_x, the effective field axis B_e is the quantization axis of the I spins, where B_e and tilt angle α are defined in Eqs. [1] and [2]. The S-spin vectors precess at a reduced coupling rate given by $J \sin \alpha$. During this precession the I-spin vectors grow along the B_e axis in proportion to $\sin \gamma$ and are maximum and of unit magnitude equal to $I^{\pm}_{max}$ when S^+ and S^- are antiparallel. (b) For ease of display, initial $2S_xI_y$, instead of $2S_yI_y$, is depicted. The preexisting I^+ and I^- vectors rotate orthogonally around B_e in the normal way at a rate of B_e Hz. The S-spin vectors precess to and fro at a coupling rate of $J \cos \phi$ where ϕ is the varying angle that the I-spin vectors make to the z axis. I^+ and I^- decrease in size in proportion to $\sin \gamma$ as S^+ and S^- precess apart. In the figure, S^+ and S^- will reverse direction when I^+ and I^- reach the $\mp y$ axes, and I^+ and I^- are depicted as having reduced in size slightly—they will increase in length back to unit magnitude when $S^{\pm}$ return again to the $\pm x$ axes. The I-spin vectors for initial $2S_yI_x$ and $2S_yI_z$ have a component aligned with the B_e axis and another orthogonal. The aligned component acts on the S-spins similarly to (a) and the orthogonal component similar to (b) with the overall time-dependent reduced coupling constant J_r being the resultant of both components—an example is provided in Fig. 4 of Ref. (*5*). Note that for clarity we have now explicitly added the magnitude of $I^{\pm}$ to the *model*, as in the discussion of Fig. 4, rather than rely on the previous implicit notion (*4, 5*) that the antiparallel spinstates are given by $\sin \gamma$.

We introduced an intuitive semiclassical vector *model* of J modulation during I-spin irradiation (*4*), applied to initial S_x, and showed that, provided $B_e \gg J$, the model was in agreement with the exact equation (f_1 in matrix [29]) derived by Anderson and Freeman using Schrödinger QM. The model was based on the previous Heisenberg vector *model* for IS pulse sequences, which had in turn been rigorously positioned within the Heisenberg QM picture (*14, 17*). In the intuitive model, the quantization axis of the I spins is assumed to be the axis of the effective field B_e, which in turn determines an instantaneous reduced coupling constant J_r acting on the S spins. The pictorial aspect of the model is displayed in Fig. 10a. The model accurately predicts the effective coupling constant during an I spin-lock field (or CW decoupling) when B_e is constant in time and also during a single adiabatic pulse in the adiabatic limit when the I-spin vectors remain aligned with a time-varying B_e field that inverts during the course of the pulse (*4*). Extensions of the model to initial $2S_yI_j$ ($j = x, y, z$) spinstates as depicted

in Fig. 10b, and to adiabatic decoupling, provided results that were nearly identical to those of exact QM simulations. The visual approach of the model guided the optimization of adiabatic decoupling schemes, often without need for detailed calculation (*5–7*). Thus, by tracking the reduced coupling constant J_r acting on the S spins during I-spin irradiation, this vector *model* has consolidated the two separate mechanisms of decoupling, mentioned above, into one picture.

The formulation of the exact QM equations, expressed in matrix [29], provides the opportunity to place this intuitive picture in a rigorous framework. The rules governing the vector *model* in the terms of our present nomenclature are:

- For initial S_x (Fig. 10a), the effective field B_e acting on the I spins determines the quantization axis (in place of the z axis in Fig. 4) such that the instantaneous coupling constant acting on the S spins is $J_r = J \sin \alpha$, where α is the normal angle of tilt of B_e from the xy plane. I-spin vectors, $I^{\pm}$, equal to the vector sum of the antiparallel spinstates, are formed along the B_e axis in proportion to sin γ, where 2γ is the angle between S^+ and S^- as a result of any coupled precession;
- For initial $2S_yI_j$ (Fig. 10b), the preexisting I-spin vectors rotate linearly about B_e in the normal way (i.e., at an angular rate of B_e Hz). The instantaneous coupling constant is given by the sine of the angle the $I^{\pm}$ vectors make to the xy plane, or $J \cos \phi$ where ϕ is the polar angle. The magnitude of the I-spin vectors decreases in proportion to sin γ, where the 2γ angle between S^+ and S^- decreases from 180° as a result of coupled precession during the irradiation.

The justification of this vector *model* is greatly facilitated by the general proof given in Section 4 that the precession of the S spins entirely depends on the orientation of the $I^{\pm}$ vectors with respect to the z axis and that, under all conditions of RF amplitude and resonance offset, the instantaneous coupling constant is $J \cos \phi$. Since this is a central premise of both of the above rules, the only remaining task is to show that the model accurately predicts the $I^{\pm}$ vectors. In the model, the effect of the $\pm J/2$ coupling fields of the S spins on the I spins is ignored, so B_e does not include a contribution from J and is defined as $B_e^2 = {B_1}^2 + \Delta H^2$. If $B_1 = 5J$, failure to include $\pm J/2$ produces an error of 0.5% in $B_e^{\pm}$ on resonance and a maximum error of 5% at about $10J$ off resonance. However, it has been noted in Sections 4 and 5 that it is difficult to predict the orientations of $I^{\pm}$ off resonance from the QM expressions without recourse to exact repetitive calculations, so the suspicion remains that larger errors might accumulate during long periods of I-spin irradiation between the vector *model* and the QM equations, even when $B_1 > 5J$.

For initial $2S_yI_j$ on resonance there is no difficulty. For initial $2S_yI_x$, the RF is on the I-spin axis, the I vectors are spin-locked, and both the vector *model* and the QM equations predict an invariant spinstate. For initial $2S_yI_y$ and $2S_yI_z$ the propeller model of Fig. 10b applies with a horizontal effective field. This is identical to the QM vector *descriptions*, as in Fig. 9, except for the 0.5% difference in cycle period corresponding to $\theta' = 360°$ and a similarly small variation in rate of rotation during each cycle given by the QM result. However, for an off-resonance comparison it has been necessary to calculate a 4×4 matrix of expressions for the vector *model* analogous to matrix [29] and to do a numerical comparison between the QM expressions and the model expressions. This showed that off resonance the vector *model* equations are accurate to better than 2% for the simultaneous combination of $B_1 > 2J$, $B_e > 3J$, and $t < (4J)^{-1}$. On average the vector *model* performs better than this because these limits represent worst cases and in cyclic applications such as adiabatic decoupling the time-length errors are repeatedly refocused. Indeed, if B_1 or $B_e > 5J$, we have found no practical applications where the limit on pulse length t causes any concern.

For initial S_x, the vector *model* assumes that the $I^{\pm}$ vectors are aligned with B_e. We have termed this the quantization axis by analogy with the z axis for coupled free precession—i.e., the vector *model* assumes that I-spin irradiation of initial S_x is an experiment that measures the equal probability of finding the I spins aligned with B_e and $-B_e$. But the QM-derived expressions in matrix [29] are inscrutably silent about the notion of a quantization axis. Again, on resonance there is no difficulty. The model depicts the quantization axis for on-resonance RF as being transverse, and so the S spins experience no coupling. This is the well-known on-resonance CW decoupling result. The relevant QM equation predicts sidebands at $\pm B_e^J$ (discussed above in relation to Eq. [43]), but these are less than 0.5% for $B_1 > 5J$ and by discarding terms in $(J/[2B_e^J])^2$ the two results agree. Although we have previously proven that a similar close correspondence arises off resonance for initial S_x and $B_e \gg J$ (*5*), it is vital for the theoretical rigor of the vector *model* that we finesse the tilted quantization axis from the exact QM expressions.

Again, a numerical approach suffices. Calculation of the antiparallel spinstates beginning with initial S_x from the terms in column 1 of matrix [29] yields

$$\text{total } I^+/I^- \text{ vectors} = 0.5(f_2^2 + f_3^2 + f_4^2)^{0.5}, \quad [57]$$

$$S_x = 0.5 * f_1 = \cos \gamma, \quad [58]$$

$$\tan \phi = f_4/(f_2^2 + f_3^2)^{0.5}, \quad [59]$$

$$\tan \beta = f_3/f_2, \quad [60]$$

where γ and ϕ are as normally defined and β is the phase angle of the transverse component of I^+ to the y axis. Typical results are shown in Fig. 11 for $B_e = 5J$. The growing I-spin vectors rapidly rotate to the B_e axis, which is at 45° tilt above the x axis, and then make small pseudo-circular precessions around this axis of about 7° amplitude indicated by the oscillations of ϕ and β. In terms of the total product operator states, the large excursions of the I-spin vectors from the B_e axis at the begin-

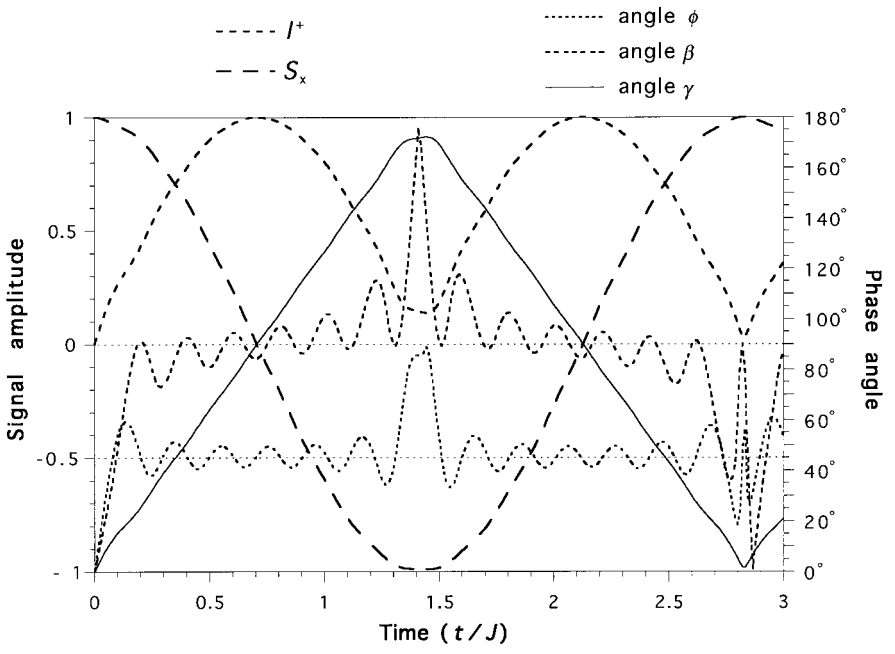

FIG. 11. Off-resonance plots of I-spin and S-spin vector positions during nonclassical rotations. Plots of the magnitude of the I-spin vectors (I^+), the angle ϕ that $I^\pm$ make to the z axis, the phase angle β of $I^\pm$ to the y axis, the magnitude of the S_x spinstate, and the angle γ, which is half the angle between S^+ and S^-. The plots are versus the length of time the I-spin irradiation is applied in units of $1/J$ s. The plots result from calculations made using Eqs. [57] to [60] assuming $B_1 = 3.5J$, $\Delta H = 3.5J$, which ensures that $B_e = 5J$. The plots would be in exact agreement with the vector model if $\phi = 45°$ (B_e at 45°) and $\beta = 90°$ throughout. Projection of the linear segments for γ onto the time axis indicates that S^+ and S^- effectively refocus at $\sqrt{2}/J$ s and $2\sqrt{2}/J$ s as expected. At the midpoint of each cycle the magnitude of the $I^\pm$ does not quite reduce to zero so that $S^\pm$ do not quite refocus on the $-x$ axis. Instead $I^\pm$ rotate rapidly and invert along the B_e axis and $S^\pm$ reverse their direction of precession. Data points used to construct the plots are not sufficient to accurately depict this rapid inversion and for ease of presentation ϕ and β are plotted as though the inversion has not occurred. Numerically, there is only a minor difference between $S^\pm$ precessing continuously through the $-x$ axis (zero $I^\pm$) or reversing just short of refocusing (very small inverting $I^\pm$).

ning, middle, and end of each cycle are when these vectors are small and so these excursions represent only a small departure from the vector *model*. Thus the I-spin vectors are almost continuously spin-locked along B_e, the postulated quantization axis, with the S-spin vectors precessing steadily at the expected reduced coupling rate, which is an average of the exact instantaneous rate given by Eq. [49].

If B_e is doubled, all excursions from the ideal vector *model* pattern are approximately halved and the quantization axis dominates. Indeed the spin-locked pattern can still be discerned for effective fields as low as $3J/2$. This pattern must inevitably break down closer to resonance, and it undergoes a dramatic change, as ΔH is reduced to $J/2$, to the cyclic $S_x \leftrightarrow 2S_yI_x$ interconversion described in Section 5. Nevertheless, we can say that, near enough, the vector *model* provides a predictive picture of I-spin irradiation of initial S_x off resonance for the simultaneous combination of $B_1 \geq J/2$ and $B_e \geq 3J/2$.

The above serves to determine the limits of analytical accuracy of the vector *model*, and the model does better than might be expected—the initial assumption that B_1 should be much greater than J tends to underestimate its striking performance relative to the more precise limits described above. However, even though it is straightforward to derive and list a complete set of analytical vector *model* equations for a 4×4 J-rotation matrix, i.e., the equivalent of matrix [29], there is no need since the exact QM matrix now exists—there are no situations in which a good approximation would be advantageous over an exact treatment when the two methods are applied in the same way and the effort of numerical calculation is similar. The unique value of this vector *model*, separate from an exact QM treatment, arises in situations where it is possible to numerically (*4*) or analytically (*5*) integrate the reduced coupling J_r over an entire amplitude/frequency-modulated RF pulse. This approach obviates the need to repeatedly apply a rotation matrix for each time increment in the pulse, and it was used to advantage in this way in the detailed analysis of adiabatic pulses (*4*) and adiabatic decoupling (*5–7*).

In addition, we now suggest that the vector *model* should be used in combination with the exact QM equations of matrix [29]. The latter are too complicated to readily convey an overall picture of IS spin behavior off resonance and it is tedious to repeatedly calculate exact vector *descriptions*. The proposition is that for B_e greater than $3J/2$, the picture is, near enough, that of the vector *model*. For $B_1 > 5J$, numerical errors in using the *model* are less than about 1–5%, so the vector picture may be considered exact. Examples of the combined use of the *model* and matrix [29] are provided in the next section.

Low RF Field Strength, $B_1 < 5J$

For field strengths less than $5J$, it is clear from the examples in Sections 4 and 5 that the QM equations of matrix [29] are required to exactly determine the behavior of an IS spin system. Apart from the pioneering work of Anderson and Freeman (*22*) and later Waugh (*23*), which yielded the equation for the f_1 term of matrix [29], there appear to have been only three other studies at low B_1 amplitude relevant to nonclassical IS rotations (*25, 28, 29*).

Henrichs and Schwartz (*28*) studied selective experiments on individual multiplet lines but did not obtain any quantitative data for nonclassical rotations. Stoll *et al.* (*29*) used the pulse sequence

$$90[\mathrm{S}]\text{–CW}[\mathrm{I}, J/2, t]\text{–}180[\mathrm{S}]\text{–}t\text{–acquire S signal,} \qquad [\mathrm{H}]$$

where CW[I, $J/2$, t] signifies RF of constant amplitude applied at a resonance offset of $J/2$ Hz for time t. The acquired S signal, which is refocused by the 180[S] pulse and the t delay, comprises only S_x and $2S_yI_z$. These are given by column 1 of matrix [29] (with a sign change of one term for the 180° pulse), multiplied by rows 1 and 4 of [41] for the t delay, to yield

$$S_x = 0.5(f_1\cos[\pi Jt] + f_4\sin[\pi Jt]); \qquad [61]$$

$$2S_yI_z = 0.5(-f_1\sin[\pi Jt] + f_4\cos[\pi Jt]). \qquad [62]$$

These simple exact equations are not in agreement with the complex expansions provided by Stoll *et al.*

A study by Davis (*25*) at low power did not discern the fundamental differences between classical and nonclassical rotations. The classical 180^J S-spin rotation was correctly identified as $S_z \rightarrow 2S_xI_z$. But the nonclassical 90^J rotation was incorrectly assumed to be $S_x \rightarrow 2S_yI_x$ ($I_y \rightarrow I_xS_x$ in the terminology used in Ref. (*25*)), instead of $S_x \rightarrow 2S_yI_y$, via 180° rotations around effective fields tilted at ±45°, by analogy with the previous work of Brondeau and Canet (*11*). It is impossible to rotate vectors around fields tilted at different angles and keep them antiparallel, so the confusion seems to have been with the expectation that the I spins originate in-phase from the $+z$ axis, as in an initial Boltzmann distribution, rather than antiparallel from $\pm z$ as required for coupled partners to the initial S-spin Boltzmann distribution. Again by analogy to classical rotations, the correct pulse amplitude and length were used but the pulses were designated as "$t\Pi$" pulses for 180° rotations of length t. These 90^J (or $t\Pi$ pulses) were employed in pairs and the offset dependence of the pairs was calculated by the method of Shaka and Keeler (*30*). That type of treatment deals exclusively with the observable signal from initial in-phase S_x magnetization and does not calculate the density matrix as a function of its complete product operator components. Thus, there would have been no opportunity to evaluate intermediate states (as expressed in matrix [29]) and observe that all magnetization was exclusively in the $2S_yI_y$ state at the midpoint between the two pulses. These pairs of 90^J pulses were used by Davis to import selectivity into the standard heteronuclear spin-echo difference experiment (*31, 32*).

A recent QM study by Zwahlen *et al.* (*33*) has the appearance of relevance to low-power calculations by claiming to provide "complete expressions describing the evolution of density terms" during adiabatic pulses applied to IS_n systems, but falls short of this goal. In transforming to a tilted frame and back again in a standard density matrix approach, Zwahlen *et al.* discarded important terms—for example, their treatment does not predict any observable S_x signal when irradiating $2S_yI_z$ and thus is more consistent with the high-power approximation expressed in matrices [42] or [56]. In acknowledging our vector *model* applied to adiabatic pulses (*4*), and in particular our concept of a reduced coupling constant, they state, "We demonstrate that a complete description of the evolution of coherences is more complex than might be anticipated on the basis of a simple scaling of the coupling constant," but later "that there is a decrease in rate at which the in-phase and antiphase components interchange." Fortunately the second notion is equivalent to a reduced coupling constant, now proven above in Section 4 for all conditions. Paradoxically, their QM treatment is not as accurate as the vector *model*, which does predict the evolution of all "coherences." Indeed, their final result that IS_n spin systems behave similarly with respect to adiabatic pulses is assured without the effort of calculation by the vector *model* in which it is assumed that if $B_e \gg J$, the S spins do not affect the I spins at all, and so their number cannot matter. But, to be precise, if the exact QM expressions of matrix [28] are used for simulations, there is an effect from the n spin number when using adiabatic pulses. For spins within about J Hz of an edge of the bandwidth, $B_e \approx J$ at the beginning or end of an adiabatic pulse and so spin number n must affect the frequency profile at the extremes of bandwidth. This will be an important factor in the design of selective narrowband adiabatic pulses when these edge effects dominate.

Zero Field Strength and a Comparison with Classical Rotations

The PO states S_x and $2S_yI_z$ are common to both the six orthogonal spinstates involved in classical rotations and the four spinstates comprising the nonclassical kind. It was noted in Section 2 that a description of classical rotations required two initial QM inputs, the Boltzmann distribution of the S spins and the equal probability of finding the coupled I spins along $\pm z$. With these two properties taken into account, the system is purely mechanical, hence classical. The more complex nature of nonclassical rotations arises because of the involvement of the transverse antiparallel states, $2S_yI_x$ and $2S_yI_y$, which are pure QM states with no mechanical analogue:

The transverse S-spin vectors comprising classical spinstates undergo free coupled (mechanical) precession in the absence of an RF field, but those of $2S_yI_x$ and $2S_yI_y$ do not. This third QM input for nonclassical rotations or transformations completely dominates at $B_1 = 0$ such that there are no rotations. With increasing RF the influence of this input weakens and rotations occur more readily and eventually become classical.

In the discussion of classical J-rotation matrix [22], the high-power approximation was mentioned but its limits were not quantified. We should use the same standard as in the discussion of nonclassical limits: If $B_1 = 5J$, failure to include $\pm J/2$ produces an error of 0.5% in $B_e^{\pm}$ on resonance and a maximum error of 5% at about $10J$ off resonance; and so the high-power approximation for classical rotations is operative for $B_1 > 5J$. This highlights a second major but related difference with nonclassical rotations: For classical rotations the passive coupled I spins are always along $\pm z$, but for nonclassical transformations the passive S spins are transverse and their variable rate of precession, which depends on the orientation of the I-spin vectors, must be assessed for B_1 fields up to $50J$. Thus, for the nonclassical kind, it would be fair to state that the rotations of the I spins become classical for $B_1 > 5J$ but the nonclassical behavior of the passive S spins persists to $50J$: This is the regime of the semi-classical vector *model*.

7. AMPLITUDE MODULATED J PULSES

New general methods can be expected from the provision of general pictorial representations of IS spin rotations at any RF power level: In Sections 2 and 5, 100% spinstate conversions have been calculated for uniform on-resonance RF of strength $B_1 \geq J/2$ and at offsets of $\pm J/2$ for more selective conversions when $B_1 < J/2$. The former can take the place of any $90°–(2J)^{-1}$ or $(2J)^{-1}–90°$ combination in any pulse sequence (*8*). The selectivity profiles of these various rectangular J pulses are given by Eqs. [26], [27], [53], and [54]. The profile for an ideal rectangular 90^J pulse (Eq. [53]; $b = 1$; $B_1 = J/2$) and the highly selective nature of this pulse, suitable for applications in protein NMR, has been demonstrated (*8*). However, simulations using Eqs. [26], [27], and [54] for the other J pulses produce large sinc wobbles off resonance typical of rectangular waveforms and generalizing the 90^J pulse to higher power also introduces these wobbles. Thus in general, rectangular J pulses are not of a standard that would be acceptable for present-day selective NMR. But by analogy with normal amplitude modulated pulses, these sinc wobbles can be suppressed by shaping J pulses. For brevity, the following summary is restricted to 180^J and 90^J pulses and concentrates mainly on the latter.

All of the calculations in the preceding sections for constant RF amplitude utilized the terms in single columns of the various rotation matrices. The calculation of the effect of amplitude modulation requires the repeated application of the appropriate rotation matrix, [22] or [29], for each rectangular

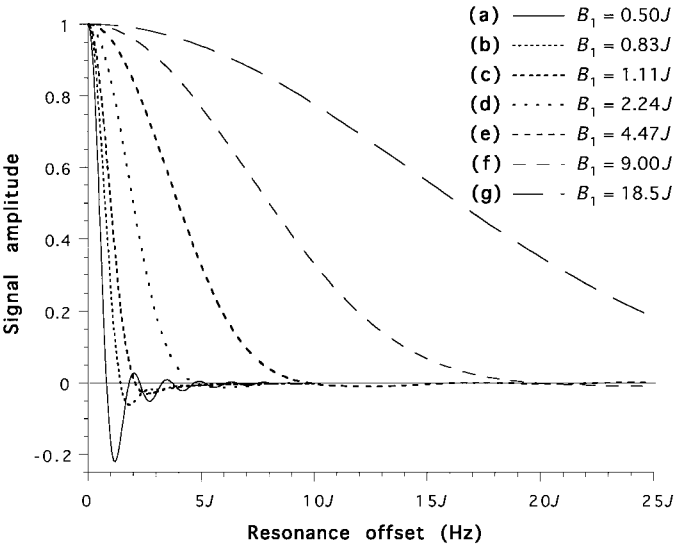

FIG. 12. Frequency offset profiles for generalized half-gaussian 90^J pulses. These were calculated by dividing the profile of the B_1 amplitude (Eq. [63]) into 100 equal time increments of constant B_1 amplitude and applying matrix [29] for each increment beginning with S_x magnetization of -1 units, i.e., $[S_x, 2S_yI_j] = [-1, 0, 0, 0]$. The signal amplitude axis corresponds to the amount of $2S_yI_y$ produced. For an assumed time t_D and $\Delta H = 0$, t_P and B_1 were obtained by iteration and values were accepted for final S_x and $2S_yI_z < 10^{-4}$ units on resonance. (a) The ideal rectangular 90^J pulse obtained by setting the truncation factor of Eq. [63] to 100% ($a = -\log 1$; $B_1 = J/2$ Hz; $t_P = (\sqrt{2}J)^{-1}$ s; $t_D = 0$). (b) A half-gaussian pulse truncated at 10% ($a = -\log 0.1$; $B_1 = 0.830J$ Hz; $t_P = 0.625J^{-1}$ s; $t_D = 0$). (c) A half-gaussian pulse truncated at 1% ($a = -\log 0.01$; $B_1 = 1.113J$ Hz; $t_P = 0.593J^{-1}$ s; $t_D = 0$). (d) As for (c) with the bandwidth at half height doubled ($t_D = 0.271J^{-1}$ s; $B_1 = 2.24J$ Hz; $t_P = 0.275J^{-1}$ s). The t_D time was inserted into the calculations with an initial application of matrix [29] for the t_D value with $B_1 = 0$. (e) As for (d) with the bandwidth doubled ($t_D = 0.387J^{-1}$ s; $B_1 = 4.47J$ Hz; $t_P = 0.136J^{-1}$ s). (f) As for (e) with the bandwidth doubled ($t_D = 0.444J^{-1}$ s; $B_1 = 9.00J$ Hz; $t_P = 0.0673J^{-1}$ s). (g) As for (f) with the bandwidth doubled ($t_D = 0.473J^{-1}$ s; $B_1 = 18.5J$ Hz; $t_P = 0.328J^{-1}$ s).

pulse increment during the pulse shape (frequency modulation requires the input of phase for each increment as in matrix [28]). Computer simulations show that, at least for simple pulse shapes like gaussian or sinc, the length t_P and the maximum B_1 amplitude, RF_{max}, can be found by iteration converging on 100% yield for a required spinstate transformation. This is true for any delay t_D between zero and $(2J)^{-1}$ s thus proving, numerically, that any classical or nonclassical spinstate transformation may be obtained with these RF shapes. The iterative search is assisted by starting with parameters for a rectangular pulse given by Eqs. [24] and [25], assuming the same average RF amplitude for the shaped and the rectangular pulse.

The mechanism of a shaped 90^J pulse on resonance is still illustrated by Figs. 5a to 5c. The $I^{\pm}$ vectors rotate to the $\pm y$ axes at a nonlinear rate, which is a combination of the nonlinear rate for a rectangular pulse and the varying rate imposed by the RF amplitude modulation. The length of the pulse is determined by the time required for $S^{\pm}$ to precess 90°, and

maximum B_1 is governed by the overall RF power to ensure 90° rotation of $I^{\pm}$—the iterative search matches these two values.

The cause and suppression of sinc wobbles for 90^J pulses can be discovered using the pictorial vector *model* established in Section 6 as being applicable for $B_e > 3J/2$ and thus resonance offsets $>3J/2$. The reason for the attenuated wobbles for the ideal rectangular pulse in Fig. 12a compared to other rectangular pulses (e.g., see Ref. (*8*)) is that, off resonance, $I^{\pm}$ are locked to B_e, B_e is tilted in the *xz* plane as in Fig. 10a, and so no $2S_yI_y$ signal is generated. The wobbles in Fig. 12a are produced to the extent that the I vectors rotate around B_e as the locking breaks down closer to resonance as discussed in relation to Fig. 11. For generalized 90^J pulses there is a mixture of S_x and $2S_yI_z$ at the beginning of the pulse. The previous remarks apply to S_x, but off resonance a component of the I vectors of $2S_yI_z$ rotates around B_e as in Fig. 10b, sinusoidally producing $2S_yI_y$ as a function of pulse length or frequency offset, hence increased wobbles.

Similar reasoning shows that shaped pulses such as gaussian or half gaussian suppress the sinc wobbles even for 90^J pulses generalized to higher power. In addition, Friedich *et al.* (*34*) have shown that the large negative side lobes (signal magnitude ≈ -0.8) produced by a normal gaussian pulse are much reduced for half-gaussian shapes, and this is also found to be true for *J* pulses. Thus, the offset profiles for the $S_x \leftrightarrow 2S_yI_y$ transformation for a series of generalized half-gaussian 90^J pulses are shown in Fig. 12. Figure 12c is the profile for a half-gaussian when there is no free precession period ($t_D = 0$) for the spinstate conversion. This has a greater bandwidth than the ideal rectangular 90^J pulse (Fig. 12a) because of the higher maximum RF amplitude, RF_{max}. The RF amplitude modulation is given by

$$B_1 = RF_{max} \exp[-a(t/t_p - 1)]^2, \qquad [63]$$

where *a* determines the truncation factor at the start of the pulse, set at the 1% level ($\log 0.01 = -a$) for Figs. 12c to 12g. Setting this factor to 100% returns a rectangular 90^J pulse as in Fig. 12a and intermediate factors produce intermediate profiles as in Fig. 12b.

Increasing RF amplitude and reducing the pulse length as a fraction of $(2J)^{-1}$ as in Figs. 12d to 12g must eventually eliminate *J* modulation as a significant factor during the pulse, and the 3×3 rotation matrix [15] again becomes applicable for simulations. Prior work has shown that the initial rectangular 90° excitation pulse in a sequence can be replaced by a gaussian (*35*) or a half-gaussian (*36*) pulse that occupies a small part of a $(2J)^{-1}$ delay and that allowance should be made for the effective period of *J*-coupled precession during the pulse, t_{eff}, where $t_{eff} + t_D = (2J)^{-1}$. However, the period t_{eff} was assumed to be $0.5t_P$ for these shaped pulses; we have not found a prior theoretical analysis that calculates this time exactly; and the connection via generalized rectangular 180^J pulses back to the work of Brondeau and Canet (*11, 12*) has not been made. Calculations using *J*-rotation matrices determine that for a gaussian shape, $t_{eff} = 0.584t_P$ at $t_D = 0$ and $t_{eff} = 0.573t_P$ for t_D close to $(2J)^{-1}$ s for both 180^J and 90^J pulses. For half-gaussian pulses the t_{eff} values are considerably changed to $(0.36 \pm 0.02)t_P$ over the full t_D range for 180^J and to $t_{eff} = (0.838 \pm 0.005)t_P$ for 90^J pulses as in Fig. 12. This result indicates that unsymmetrical 90^J pulses will have the advantage of increasing $(2J)^{-1}$ s periods by the smallest proportion when inserted into pulse sequences. Overall, these simulations also show that using the assumption made by Kessler and co-workers (*35, 36*) that $t_{eff} = 0.5t_P$, simple shaped pulses designed for single spin rotations can be substituted for any 90° pulse in a sequence with less than 10% loss in *S*/*N* on resonance provided that t_{eff} is less than or about half of $(2J)^{-1}$ s. This loss can then be eliminated by experimental adjustment of t_D and RF_{max} and the actual offset profile for the pulse will be very similar to that for a single spin with the same RF_{max}.

This conclusion would seem to obviate the need for exact analyses of semi-selective 90° pulses in cases when the bandwidth at half height is about $3J$ or more. However, if a bandwidth greater than $2J$ is chosen, the nominal t_D period for a simple shape such as half-gaussian can be used for the application of an additional period of modulated RF to obtain a squarer selectivity profile. An example is provided in Fig. 13, where a half one-lobe sinc calibrated for $t_D = (4J)^{-1}$ has been replaced by a half three-lobe sinc for which $t_D = 0$.

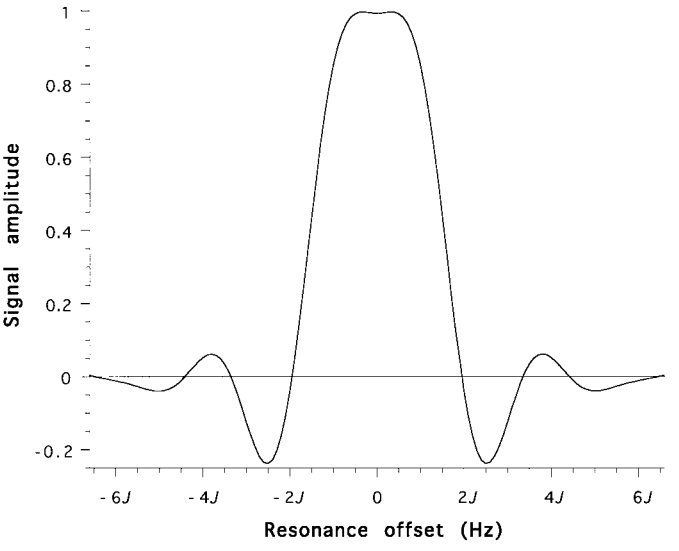

FIG. 13. Frequency offset profile for an optimized half three-lobe sinc 90^J pulse. The profile for a half three-lobe sinc was calculated similarly to those in Fig. 12 assuming $t_D = 0$. By iteration it was found that the squareness of the profile could be improved by doubling the amplitude of the minor initial lobe with the conditions for the overall pulse given by $RF_{max} = 1.8J$ and $t_P = 0.58J^{-1}$.

8. CONCLUSIONS

A weakly coupled two-spin system is central to high-resolution NMR because almost all pulse sequences used for the elucidation of molecular structure depend on the transfer of information between nuclear spins via the scalar coupling. This study provides a comprehensive survey of the analytical forms for the orthogonal states produced from any initial product operator IS spinstate under arbitrary RF conditions applied to one spin (*1*). The complete set of exact equations encompasses all previous research on a two-spin system and is applicable to homonuclei and heteronuclei.

The analysis clearly separates two kinds of spin rotations or transformations that we have described above as classical or nonclassical. The first kind can be considered as including all spinstate interconversions except those involving the antiparallel transverse states, $2S_xI_x$, $2S_yI_x$, $2S_xI_y$, or $2S_yI_y$. Two QM assumptions are required for the initial conditions prior to a classical rotation: The magnetization of one of the spins was derived from a thermal Boltzmann distribution; and one of the spins has an equal probability of being found along $\pm z$. During the rotations, no further QM principles are needed, and the result can be exactly determined as the classical rotation of the magnetizations of one spin about two effective fields, which are the resultant of B_1, resonance offset, and the $\pm J/2$ coupling fields of the other spin along $\pm z$. Various spinstate transformations that occur in 100% yield can be found from this vector *model* or from the corresponding equations. For $B_1 > 5J$ the influence of scalar coupling during the RF irradiation can be neglected: the high-power approximation is operative.

Nonclassical rotations always include the transverse antiparallel states, either transiently or as an initial or final state. Thus, for irradiation of an I spin, the nonclassical kind involves interconversions of the four spinstates, S_x, $2S_yI_x$, $2S_yI_y$, and $2S_yI_z$. The nonclassical behavior arises from the well-known invariance in time of the $2S_yI_x$ and $2S_yI_y$ spinstates when $B_1 = 0$, which is strictly quantum mechanical. Within the Heisenberg picture of quantum mechanics, for example, this phenomenon is ascribed to the physical concept that whenever one of the IS spins flips its orientation in the transverse plane, the other spin must also flip (*14, 20, 21*). The nonlinear RF-induced rotations for small B_1 are dominated by such QM effects from the correlated spins, but these effects become less important with increasing RF field. At intermediate strengths, corresponding to $5J \leq B_1 \leq 50J$, a semi-classical vector *model* (*4, 5*) can be employed with a high degree of accuracy in which the rotations of the I spins are classical or they are spin-locked. At all field strengths, the passive S spins precess via a reduced coupling constant that is exactly determined by the cosine of the polar angle of the I-spin vectors. For $B_1 > 50J$ the I-spin rotations may be considered to be instantaneous with no significant S-spin precession from coupling during the application of RF to the I spins.

At low power, vector *descriptions*, obtained by tracking the I- and S-spin magnetizations in time using the QM equations, are helpful in analyzing the 100% spinstate conversions available via nonclassical rotations. Taken together with the classical transformations, the overall analysis yields a general means of substituting frequency-selective pulses into existing pulse sequences. Potentially, by utilizing J-modulated precession during selective pulses, any combination of a 90° pulse and a $(2J)^{-1}$ period in any pulse sequence can be replaced with a shaped selective pulse of any bandwidth. One important result is that, provided that the length of the shaped 90° pulse is approximately half the length of the $(2J)^{-1}$ period or less, selective pulses that have been calibrated for single spin excitation can be inserted directly in place of any 90° pulse in a sequence. The modest loss of S/N resulting from the single spin assumption can be regained by experimental calibration. However, the remainder of the delay period may be used to impose a longer RF pulse and so improve the squareness of the off-resonance profile at the selected bandwidth—for nonclassical rotations, this concept is guided by the vector *description* on resonance and the vector *model* off resonance. These pulses may be designed by numerical simulation using the analytical forms of Eqs. [22] and [29] or the more efficient algorithms of Ref. (*1*).

Beginning with the work of Freeman and coauthors on J-coupled evolution 2 decades ago (*37, 38*), vector pictures have played a major role in the invention of the fundamental units of heteronuclear pulse sequences: for example, various spin-echo methods (e.g., *31, 32*); INEPT (*38*); the basic four-pulse HMQC sequence (*20*); and the IS spin version of DEPT (*20*). Physical pictures, such as the Heisenberg vector model (*14*), combined the notion of classical rotations at high power with quantum mechanical principles at zero power (to cope with the transverse antiparallel states) to provide an overall semi-classical description of heteronuclear experiments. These physical descriptions were less important in the development of coupled homonuclear experiments because of the added complexity of the numerous signal pathways generated by simultaneous I/S pulses, but are still valid, as illustrated by Freeman (*19*). Recently we extended the ambit of IS spin vector pictures with the semi-classical *model* that is applicable to adiabatic pulses and decoupling at intermediate power levels (*4, 5*). The comparison of these vector *models* with calculations of *measurable* magnetization vectors using exact QM equations, presented here, shows that these pictorial *models* cover the entire range of IS spin experiments except any RF-induced rotations involving the transverse antiparallel states at low power in the range $0 < B_1 < 5J$. The evolution of I- and S-spin magnetizations in this modest region can be calculated directly from the analytical equations or envisaged from the various examples illustrated in the figures in this article, so providing a continuum of physical pictures over all possible conditions. These pictures comply with an accelerating trend toward a "visual language" which, according to Horn (*39*), is

more efficient in summarizing data and conveying complex ideas.

REFERENCES

1. T. E. Skinner and M. R. Bendall, *J. Magn. Reson.* **141,** 271 (1999).
2. G. A. Morris and R. Freeman, *J. Magn. Reson.* **29,** 433 (1978).
3. J.-M. Bernassau and J.-M. Nuzillard, *J. Magn. Reson. A* **104,** 212 (1993).
4. M. R. Bendall, *J. Magn. Reson. A* **116,** 46 (1995).
5. T. E. Skinner and M. R. Bendall, *J. Magn. Reson.* **134,** 315 (1998).
6. M. R. Bendall and T. E. Skinner, *J. Magn. Reson.* **129,** 30 (1997).
7. M. R. Bendall and T. E. Skinner, *J. Magn. Reson.* **134,** 331 (1998).
8. M. R. Bendall and T. E. Skinner, *J. Magn. Reson.* **141,** 261 (1999).
9. M. R. Bendall and D. T. Pegg, *Magn. Reson. Med.* **2,** 91 (1985); M. R. Bendall and D. T. Pegg, *J. Magn. Reson.* **63,** 494 (1985); M. R. Bendall and D. T. Pegg, *J. Magn. Reson.* **66,** 546 (1986).
10. O. W. Sorensen, G. W. Eich, M. H. Levitt, G. Bodenhausen, and R. R. Ernst, *Progr. NMR Spectrosc.* **16,** 163 (1983); F. J. M. van de Van and C. W. Hilbers, *J. Magn. Reson.* **54,** 512 (1983); K. J. Packer and K. M. Wright, *Mol. Phys.* **50,** 797 (1983).
11. J. Brondeau and D. Canet, *J. Magn. Reson.* **47,** 419 (1982).
12. D. Canet, J. Brondeau, J. P. Marchal, and H. Nery, *J. Magn. Reson.* **36,** 35 (1979).
13. R. Bazzo and J. Boyd, *J. Magn. Reson.* **79,** 568 (1988).
14. D. T. Pegg, M. R. Bendall, and D. M. Doddrell, *J. Magn. Reson.* **44,** 238 (1981).
15. A. A. Chalmers, K. G. R. Pachler, and P. L. Wessels, *J. Magn. Reson.* **15,** 415 (1974); H. J. Jakobsen, P. J. Kanyha, and W. S. Brey, *J. Magn. Reson.* **54,** 134 (1983); and references contained therein.
16. H. Bildsoe, *J. Magn. Reson.* **27,** 393 (1977).
17. M. R. Bendall, D. T. Pegg, and D. M. Doddrell, *J. Magn. Reson.* **45,** 8 (1981).
18. J. Shriver, *Concepts Magn. Reson.* **4,** 1 (1992).
19. R. Freeman, *Concepts Magn. Reson.* **10,** 63 (1998).
20. M. R. Bendall, D. T. Pegg, and D. M. Doddrell, *J. Magn. Reson.* **52,** 81 (1983).
21. M. R. Bendall, D. T. Pegg, D. M. Doddrell, and D. M. Thomas, *J. Magn. Reson.* **46,** 43 (1982).
22. W. A. Anderson and R. Freeman, *J. Chem. Phys.* **37,** 85 (1962).
23. J. S. Waugh, *J. Magn. Reson.* **49,** 517 (1982).
24. M. R. Bendall and T. E. Skinner, *J. Magn. Reson.* **139,** 175 (1999).
25. D. G. Davis, *J. Magn. Reson. B* **101,** 229 (1993).
26. M. H. Levitt, G. Bodenhausen, and R. R. Ernst, *J. Magn. Reson.* **53,** 443 (1983).
27. C. P. Slichter, "Principles of Magnetic Resonance," 3rd ed., p. 306, Springer-Verlag, New York (1990).
28. P. M. Henrichs and L. J. Schwartz, *J. Magn. Reson.* **28,** 477 (1977).
29. M. E. Stoll, A. J. Vega, and R. W. Vaughan, *J. Chem. Phys.* **67,** 2029 (1977); M. Stoll, A. J. Vega, and R. W. Vaughan, *Phys. Rev. A* **16,** 1521 (1977).
30. A. J. Shaka and J. Keeler, *Prog. NMR Spectrosc.* **19,** 47 (1987).
31. M. R. Bendall, D. T. Pegg, D. M. Doddrell, and J. Field, *J. Am. Chem. Soc.* **103,** 934 (1981).
32. R. Freeman, T. H. Mareci, and G. A. Morris, *J. Magn. Reson.* **42,** 341 (1981).
33. C. Zwahlen, S. J. F. Vincent, and L. E. Lewis, *J. Magn. Reson.* **130,** 169 (1998).
34. J. Friedrich, S. Davies, and R. Freeman, *J. Magn. Reson.* **75,** 390 (1987).
35. H. Kessler, H. Oschkinat, and C. Griesinger, *J. Magn. Reson.* **70,** 106 (1986).
36. H. Kessler, U. Anders, G. Gemmecker, and S. Steuernagel, *J. Magn. Reson.* **85,** 1 (1989).
37. R. Freeman, *Bull. Magn. Reson.* **1,** 5 (1979).
38. G. A. Morris and R. Freeman, *J. Am. Chem. Soc.* **101,** 760 (1979).
39. R. E. Horn, "Visual Language," Macro VU Press, Bainbridge Island, WA (1998).